Behavioral/Cognitive

# Bacteria-Derived Peptidoglycan Triggers a Noncanonical Nuclear Factor-κB-Dependent Response in *Drosophila* Gustatory Neurons

**Ambra Masuzzo,[1*] Gérard Manière,[2*] Yaël Grosjean,[2] Léopold Kurz,[1] and Julien Royet[1]**

[1]Centre National de la Recherche Scientifique, Aix-Marseille Université, Institut de Biologie du Developpement de Marseille, 13009 Marseille, France, and [2]Centre National de la Recherche Scientifique; Institut National de Recherche pour l'Agriculture, l'Alimentation et l'Environnement; Université Bourgogne Franche-Comté, Centre des Sciences du Goût et de l'Alimentation, L'Institut Agro Dijon, Dijon 21000, France

**Probing the external world is essential for eukaryotes to distinguish beneficial from pathogenic micro-organisms. If it is clear that the main part of this task falls to the immune cells, recent work shows that neurons can also detect microbes, although the molecules and mechanisms involved are less characterized. In *Drosophila,* detection of bacteria-derived peptidoglycan by pattern recognition receptors of the peptidoglycan recognition protein (PGRP) family expressed in immune cells triggers nuclear factor-κB (*NF-κB*)/immune deficiency (IMD)-dependent signaling. We show here that one PGRP protein, called PGRP-LB, is expressed in bitter gustatory neurons of proboscises. *In vivo* calcium imaging in female flies reveals that the PGRP/IMD pathway is cell-autonomously required in these neurons to transduce the peptidoglycan signal. We finally show that NF-κB/IMD pathway activation in bitter-sensing gustatory neurons influences fly behavior. This demonstrates that a major immune response elicitor and signaling module are required in the peripheral nervous system to sense the presence of bacteria in the environment.**

*Key words:* **bacteria; *Drosophila*; gustatory neurons; *NF-κB*; peptidoglycan**

**Significance Statement**

**In addition to the classical immune response, eukaryotes rely on neuronally controlled mechanisms to detect microbes and engage in adapted behaviors. However, the mechanisms of microbe detection by the nervous system are poorly understood. Using genetic analysis and calcium imaging, we demonstrate here that bacteria-derived peptidoglycan can activate bitter gustatory neurons. We further show that this response is mediated by the PGRP-LC membrane receptor and downstream components of a noncanonical NF-κB signaling cascade. Activation of this signaling cascade triggers behavior changes. These data demonstrate that bitter-sensing neurons and immune cells share a common detection and signaling module to either trigger the production of antibacterial effectors or to modulate the behavior of flies that are in contact with bacteria. Because peptidoglycan detection doesn't mobilize the known gustatory receptors, it also demonstrates that taste perception is much more complex than anticipated.**

Received Dec. 13, 2021; revised July 13, 2022; accepted July 15, 2022.

Author contributions: A.M., G.M., Y.G., L.K., and J.R. designed research; A.M., G.M., and L.K. performed research; G.M. contributed unpublished reagents/analytic tools; A.M., G.M., Y.G., L.K., and J.R. analyzed data; A.M., G.M., Y.G., L.K., and J.R. wrote the paper.

This work was supported by Agence Nationale de la Recherche Grants ANR-11-LABX-0054, ANR-17-CE16-0023-01, and ANR-18-CE15-0018-02; Fondation pour la Recherche Médicale Grant EQU201903007783; and l'Institut Universitaire de France (J.R.). Y.G. was supported by the Centre National de la Recherche Scientifique, Université de Bourgogne Franche-Comté, Conseil Régional Bourgogne Franche-Comte (PARI grant), European Funding for Regional Economical Develoment, and European Council Grant GliSFCo-311403. We thank Emilie Avazeri and Annelise Viallat-Lieutaud for technical help and members of the Royet laboratory for comments on the manuscript.

*A.M. and G.M. share senior authorship.

The authors declare no competing financial interests.

Correspondence should be addressed Julien Royet at Julien.royet@univ-amu.fr or Léopold Kurz at leo.kurz@univ-amu.fr or Yaël Grosjean at yael.grosjean@cnrs.fr.

https://doi.org/10.1523/JNEUROSCI.2437-21.2022



## Introduction

Because micro-organisms can reduce the fitness of their hosts, natural selection has favored defense mechanisms that protect them against disease-causing agents. The molecular mechanisms that are activated during the humoral and cellular responses, the main armed branches of the host against invading microbes, are known in great detail. By avoiding pathogenic microorganisms or modifying its behavior when infected, the host can prevent the activation of the costly immune response, maximize its efficiency, and reduce the consequences of the infection on itself or its progeny. Phenotypes related to such behaviors are well known in mammals. They range from disgust to social isolation including sleepiness (Kavaliers et al., 2020). These responses to the microbial environment are accepted as symptoms but are not well

defined molecularly. Observations in invertebrates phenocopying the mammalian sickness behaviors have also been made (Sullivan et al., 2016) and may often be interpreted in an anthropomorphic way while there is no molecular deciphering or ecological context. For instance, social insects, such as termites, can ascertain the virulence of the *Metarhizium* and *Beauveria* fungi and avoid the most virulent strains (Mburu et al., 2009), whereas *Apis mellifera* workers are able to detect larvae infected with the fungus *Ascosphaera apis* and remove them from the nest (Swanson et al., 2009). On the other hand, as some microorganisms are beneficial for their host, animals can also be attracted by them. To date, the molecular and neuronal basis of these behavioral responses to microbes are much less characterized than the canonical immune responses. Genetically tractable models such as *Caenorhabditis elegans* or *Drosophila melanogaster* are very well suited to elucidate them (Aranha and Vasconcelos, 2018; Sayin et al., 2018; Hoffman and Aballay, 2019; Masuzzo et al., 2020).

Devoid of adaptative immunity like all invertebrates, *Drosophila* has emerged as a well-adapted model to unravel the signaling modules that control the innate immune responses against bacteria (Buchon et al., 2014; You et al., 2014; Martino et al., 2017; Zhai et al., 2018b). Essential to them are two nuclear factor (NF)-$\kappa$B signaling pathways called Toll and immune deficiency (IMD), whose activation triggers the production of immune effectors, such as antimicrobial peptides (AMPs), in immune-competent cells (De Gregorio et al., 2002; Lindsay and Wasserman, 2014; Myllymaki et al., 2014; Zhai et al., 2018b). This activation depends on the previous detection of bacteria-derived peptidoglycan (PGN) by host pattern recognition receptors (PRRs) belonging to the peptidoglycan recognition protein (PGRP) family (Royet et al., 2011; Kurata, 2014). Previous work has shown that signaling components of the NF-$\kappa$B/IMD pathway, including the NF-$\kappa$B transcription factor Relish, and the upstream PGRP sensors are functionally required outside the immune system and more specifically in some neurons of the CNS (Kurz et al., 2017; Kobler et al., 2020). Direct recognition of circulating bacteria-derived PGN by few brain octopaminergic neurons leads to their inhibition and, in turn, to an egg-laying reduction in PGN-exposed females (Masuzzo et al., 2019; Kobler et al., 2020). Hence, by detecting a ubiquitous bacteria cell wall component via dedicated PRRs, few brain neurons adapt the female physiology to its infectious status.

The peripheral nervous system (PNS) of *Drosophila* and more specifically its gustatory and olfactory systems are also involved in microbe-induced behaviors. By activating a subclass of olfactory neurons that express the olfactory receptor Or56a, the microbial odorant geosmin induces pathogen avoidance by inhibiting oviposition, chemotaxis, and feeding (Stensmyr et al., 2012). In contrast, bacterial volatiles commonly produced during decomposition of plant material such as ammonia and certain amines are highly attractive to flies (Min et al., 2013). Furthermore, Or30a-dependent detection of bacteria-derived short-chain fatty acid induces attraction in larvae (Depetris-Chauvin et al., 2017). Previous works demonstrated that bacterial cell wall components like lipopolysaccharide (LPS) and PGN are detected by the *Drosophila* gustatory sensory system (Yanagawa et al., 2017). Detection of LPS by the esophageal bitter gustatory receptor neurons (GRNs) expressing the chemosensory cation channel TrpA1 (transient receptor potential cation channel subfamily A member 1) triggers feeding and oviposition avoidance (Soldano et al., 2016). PGN detection, instead, triggers grooming behavior on stimulation of wing margins and legs, but the nature of gustatory sensory neurons and receptors involved in this behavior remain elusive (Yanagawa et al., 2017).

Previous work has shown that recognition of bacteria-derived PGN by fly PGRPs mediates many of these procaryotes–eucaryotes interactions. Diamino pimelic PGN (DAP-type PGN) found in the cell wall of most Gram-negative bacteria is detected either at the membrane of immune competent cells by PGRP-LC or in the cytosol by the soluble PGRP-LE receptor (Leulier et al., 2003; Kaneko et al., 2006; Charroux et al., 2018). In both cases, this recognition step is sufficient to activate the evolutionary conserved NF-$\kappa$B downstream signaling cascade, which, in turn, will induce the production of antibacterial molecules. Probably because its prolonged activation is detrimental for the host, NF-$\kappa$B pathway activation levels are finely modulated by several negative regulators (Lee and Ferrandon, 2011). Among them are enzymes, called amidases, which by binding and cleaving the PGN into inactive products buffer IMD pathway activation. PGRP-LB is such an enzyme that is present either extracellularly via its PGRP-LB$^{RC}$ isoform or inside the cell via the PGRP-LB$^{RA}$ and $^{RD}$ isoforms (Charroux et al., 2018). We present here data demonstrating that the PGRP-LB enzyme and other IMD pathway components are expressed in some gustatory neurons, suggesting that these cells might sense and react to external PGN. Using genetic analysis and calcium imaging, we demonstrate that some members of the IMD pathway are functionally required in bitter-sensing gustatory neurons to sense and transduce the presence of PGN without the mobilization of the classical gustatory receptors expressed in these cells. These results demonstrate that the taste system can be used by the fly to detect the presence of PGN in the environment and that the PGRP/IMD module is not only required in immune cells to trigger the production of antibacterial effectors but also in sensory neurons to modulate fly behavior on bacteria sensing. Thus, the PGN that is used as an alarm signal when detected within the body cavity is as well a qualitative readout about the fly environment.

## Materials and Methods

*Experimental designs*

*Fly stocks.* Detailed genotypes of all the flies used can be found at https://figshare.com/articles/online_resource/Raw_data_and_statistics_for_each_figure_xlsx/20160395.

All flies (only females were used in this study) were maintained at 25°C on a standard cornmeal/agar medium on a 12 h light/dark cycle with a relative humidity of 70%. The strains used are the following: pLB1$^{Gal4}$ (Kurz et al., 2017), PGRP-LB::GFP (Masuzzo et al., 2019), *w* [stock #3605, Bloomington Drosophila Stock Center (BDSC)], *yw*, *Canton-S*, Gr5a$^{LexA}$ (Mishra et al., 2013; Kim et al., 2018; provided by Dong Min Shin), Gr66a$^{LexA}$ (Thistle et al., 2012; provided by K. Scott lab), Gr32a$^{LexA}$ (Fan et al., 2013; provided by A. Dahanukar lab), Gr32a$^{Gal4}$ (stock #57622, BDSC), Gr66a$^{Gal4}$, Gr66a-RFP(X4;BDSC:60 691), UAS-TrpA1 (stock #26264, BDSC; Hardie et al., 2001), UAS-Kir2.1 (stock #6595, BDSC), 40XUAS-mCD8-GFP (stock #32195, BDSC), UAS-Fadd RNAi (Khush et al., 2002), UAS-Imd RNAi [stock #101834, Vienna Drosophila Resource Center (VDRC)], UAS-Dredd RNAi (stock #104726, VDRC), UAS-PGRP-LC RNAi (stock #101636, VDRC), UAS-Relish RNAi (stock #28943, BDSC), UAS*frt*STOP*frt* mCD8GFP (stock #30125, BDSC), 8XLexAop2-FLP (stock #55819, BDSC), UAS-GCaMP6s (stock #42746, BDSC), UAS-PGRP-LCa (Maillet et al., 2008), *PGRP-LC*$^{E12}$ (Gottar et al., 2002), *PGRP-LE*$^{112}$ (Takehana et al., 2004), *PGRP-LB*$^{ko}$ (Paredes et al., 2011), *Dredd*$^{D55}$ (Leulier et al., 2000), and *dTrpA1*$^{1}$ (Soldano et al., 2016).

*Tastants*

For *in vivo* calcium imaging and flyPAD assays, tastants were dissolved in autoclaved purified distilled water. All tastant solutions were freshly prepared and stored in aliquots at −20°C for a maximum duration of 6 months. Peptidoglycan was obtained from InvivoGen (PGN-EK, catalog #tlrl-pgnek), sucrose *from Carl Roth* (catalog #4621.1), and caffeine from Sigma-Aldrich (catalog #C0750).

In vivo *calcium imaging*

*In vivo* calcium imaging experiments were performed on 5–7 d-old starved mated females. Animals were raised on conventional media with males at 25°C. Flies were starved for 20–24 h in a tube containing a filter soaked in water prior to any experiments. Flies of the appropriate genotype were anesthetized on ice for 1 h. Female flies were suspended by the neck on a Plexiglas block (2 × 2 × 2.5 cm), with the proboscis facing the center of the block. Flies were immobilized using an insect pin (0.1 mm diameter) placed on the neck. The ends of the pin were fixed on the block with beeswax (Deiberit 502, catalog #209212, Siladent). The head was then glued on the block with a drop of rosin (Gum rosin, catalog #60895, Sigma-Aldrich) dissolved in ethanol at 70%) to avoid any movements. The anterior part of the head was thus oriented toward the objective of the microscope. Flies were placed in a humidified box for 1 h to allow the rosin to harden without damaging the living tissues. A plastic coverslip with a hole corresponding to the width of the space between the two eyes was placed on top of the head and fixed on the block with beeswax. The plastic coverslip was sealed on the cuticle with two-component silicon (Kwik-Sil, World Precision Instruments) leaving the proboscis exposed to the air. Ringer's saline containing the following (in mM) 130 NaCl, 5 KCl, 2 $MgCl_2$, 2 $CaCl_2$, 36 saccharose, 5 HEPES, pH 7.3, was placed on the head (Silbering et al., 2012). The antenna area, air sacs, and the fat body were removed. The gut was cut without damaging the brain and taste nerves to allow visual access to the anterior ventral part of the subesophageal zone (SEZ). The exposed brain was rinsed twice with Ringer's saline. GCaMP6s fluorescence was viewed with a Leica DM600B microscope under a 25× water objective. GCaMP6s was excited using a Lumencor diode light source at 482 nm ± 25. Emitted light was collected through a 505–530 nm bandpass filter. Images were collected every 500 ms using a Hamamatsu/HPF-ORCA Flash 4.0 camera and processed using Leica MM AF software version 2.2.9. Stimulation was performed by applying 140 µl of tastant solution diluted in water on the proboscis. For *Escherichia coli* K12 stimulation, bacteria were grown in LB media overnight at 37°C, spined down 10 min at 3500 × *g* and the pellet suspended in water to obtain a final optical density (OD)600 of 0.5. A minimum of two independent experiments with a total number for each condition ranging from 7 to 10 were performed. Each experiment consisted of recording 10 images before stimulation and 30 images after stimulation. Data were analyzed as previously described using Fiji software (https://fiji.sc/; Silbering et al., 2012). In all experiments implicating $pLB1^{Gal4}$, this driver and the UAS-GCaMP6s transgenes are homozygous. In experiments using $Gr66a^{Gal4}$, the driver and the UAS-GCaMP6s transgenes are heterozygous.

*Immunostaining and imaging*

Immunostaining and imaging were performed as previously described (Masuzzo et al., 2019). Brains from adult females were dissected in PBS (catalog #CS0PBS0108, Eurobio Scientific) and fixed for 15 min in 4% paraformaldehyde (catalog #15714-S, Electron Microscopy Sciences) at room temperature (RT). Afterward, brains were washed three times for 10 min in PBS-T (PBS + 0.3% Triton X-100) and blocked in 2.5% bovine serum albumin (BSA; Sigma-Aldrich) in PBS-T for 30 min. After saturation, samples were incubated with the primary antibody diluted in 0.5% BSA in PBS-T overnight at 4°C. The following day, brains were washed three times and incubated with the secondary antibody diluted in 0.5% BSA in PBS-T for 2 h at RT. Next, samples were washed for 10 min in PBS-T and mounted on slides using Vectashield (Vector Laboratories) fluorescent mounting medium. In the case of proboscises, no immunostaining was performed. Proboscises of adult females were dissected in PBS, rinsed with PBS, and directly mounted on slides using Vectashield fluorescent mounting medium. The tissues were visualized directly after.

For the immunostaining the primary antibodies used are the following: Chicken anti-GFP (1:1000; catalog #GFP-1020, Aves Labs; RRID:AB_10000240), rabbit anti-RFP (1:1000; catalog #600–401-379, Rockland; RRID:AB_2209751), and mouse anti-nc82 (1:40; catalog #nc82, Developmental Studies Hybridoma Bank; RRID:AB_2314866). The secondary antibodies used are the following: Alexa Fluor 488 Donkey anti-Chicken IgY (IgG) (H + L; 1:500; catalog #703-45-155, Jackson ImmunoResearch; RRID:AB_2340375), Alexa Fluor 568 donkey anti-mouse IgG (H + L; 1:500; catalog #A10037, Thermo Fisher Scientific; RRID:AB_2534013), Alexa Fluor 647 donkey anti-mouse IgG (H + L; 1:500; catalog #715-605-151, Jackson ImmunoResearch; RRID:AB_2340863), and Alexa Fluor 568 donkey anti-rabbit IgG (H + L; 1:500; catalog #A10042, Thermo Fisher Scientific; RRID: AB_2534017).

Images were captured with either a Leica SP8 confocal microscope (in this case, tissues were scanned with 20× oil immersion objective) or an LSM 780 Zeiss confocal microscope (20× air objective was used). For the detection of endogenous PGRP-LB::GFP, images were captured with a Spinning Disk Ropper 2 Cam (20× or 40× air objective were used). Images were processed using Adobe Photoshop.

*Feeding assay*

Mated females 5–7 d-old were used. Animals were starved as a group for 20 h at 25°C before the assay in a tube containing a filter soaked in water. Previously, these females were raised with males on a conventional media at 25°C or 29°C for RNAi experiments. The assay could not last >1 h as the food is totally consumed after this period. Two-choice feeding assays were performed by using the flyPAD device (Itskov et al., 2014), which records the cumulative number of sips. Each sip corresponds to a contact of the proboscis of the flies with the chosen food substrate. Individual flies were captured via aspiration (neither $CO_2$ nor ice used) and deposited in arenas containing two food substrates. The control substrate consisted of a 1% agarose 5 mM sucrose solution, whereas the test substrate additionally contained peptidoglycan dissolved in water at the indicated concentrations. The wells of each arena (two per arena) were filled with 3.5 µl of food solution. Tests were run for 1 h at 25°C under constant light in a behavioral room limiting the influence of external light and noise. Data were collected and analyzed using Bonsai (Lopes et al., 2015) and MATLAB, respectively (scripts provided by Pavel Itskov). Preference index was calculated as follows: (number of sips in the test solution − number of sips in the control solution)/total number of sips. Noneaters were excluded from the analysis.

*Oviposition assay*

Oviposition assays were performed as previously described (Masuzzo et al., 2019). Mated females 5 d-old were used and raised on conventional media with males. Eclosed flies were raised at 25°C or 21°C, in case of experiments involving the thermosensitive transgene UAS-TrpA1 or 29°C for RNAi experiments. Mated females 5 d-old were anesthetized on a $CO_2$ pad and singularly transferred in tubes containing a fresh (not older than 48 h) conventional media with some dry yeast (Fermipan) on top of it right before the egg-laying period. Flies were let to lay eggs for 24 h at 25°C or 23°C in control conditions for experiments involving UAS-TrpA1 or 29°C for test conditions for experiments involving UAS-TrpA1 and RNAi experiments. After the egg-laying period, animals were discarded, and eggs were counted using a binocular scope. At least two independent trials with at least 20 females per trial, genotype, and condition were used.

*Statistical analysis in vivo calcium imaging*

The D'Agostino–Pearson test to assay whether the values are distributed normally was applied. As not all the datasets were considered normal, nonparametric statistical analysis such as nonparametric unpaired Mann–Whitney two-tailed tests or nonparametric unpaired ANOVA, Kruskal–Wallis test, and Dunn's post-test were used for all the data presented.

*Feeding assay*

The D'Agostino–Pearson test to assay whether the values are distributed normally was applied. As not all the datasets were considered normal, nonparametrical statistical analysis such as nonparametric unpaired Mann–Whitney two-tailed tests or nonparametric unpaired ANOVA, Kruskal–Wallis test, and Dunn's post-test were used for all the data presented.

*Oviposition assay*

The D'Agostino–Pearson test to assay whether the values are distributed normally was applied. As not all the datasets were considered normal, nonparametrical statistical analysis and specifically the nonparametric unpaired ANOVA, Kruskal–Wallis test, and Dunn's post-test were used for all the data presented.

GraphPad Prism 8 software was used for statistical analyses.

Detailed statistical analyses, raw data, and population sizes can be found at https://figshare.com/articles/online_resource/Raw_data_and_statistics_for_each_figure_xlsx/20160395.

## Results

### A peptidoglycan-binding protein is expressed in some bitter gustatory neurons

Our previous work has shown that some PGN sensing molecules (PGRPs) are active outside immune cells and specifically in neurons of the CNS. Indeed, the direct detection of bacteria-derived PGN by the cytosolic protein PGRP-LE in a subset of brain octopaminergic neurons modulates oviposition of infected females in an NF-κB-dependent manner (Kurz et al., 2017; Masuzzo et al., 2019). To identify neurons that potentially expressed PGRPs and thus respond to PGN, we previously made use of a reporter line, pLB1$^{Gal4}$, that partially recapitulates the endogenous expression of one PGRP-LB protein isoform (i.e., PGRP-LB$^{RD}$; Masuzzo et al., 2019). We now noticed that in addition to being expressed in some neurons of the brain, this line also labeled axonal projections that originated from neurons of the PNS. In pLB1$^{Gal4}$/UAS-mCD8-GFP flies, a GFP signal was observed in the SEZ of the central brain where GRNs send their axonal projections (Fig. 1*a*,*b*; Marella et al., 2006; Kwon et al., 2014). Accordingly, some spare cell bodies present in the labella at the position of taste sensory neurons were detected (here called pLB1+ neurons; Figs. 1*c*, 2, Table 1) (Montell, 2009; Weiss et al., 2011; French et al., 2015; Chen and Dahanukar, 2020). In contrast, no signal was detected using the two other PGRP-LB isoform reporter constructs pLB2$^{Gal4}$ and pLB3$^{Gal4}$ (Fig. 2; Kurz et al., 2017). The axonal network within the SEZ of pLB1$^{Gal4}$/UAS-mCD8-GFP flies is reminiscent of taste neurons associated with detection of molecules triggering aversion and classified as bitter. Double staining between pLB1$^{Gal4}$/UAS-mCD8-GFP and Gr66a-RFP, which is specifically expressed in bitter gustatory neurons, revealed that all pLB1+ neurons are bitter (Gr66a+), although they only represent a subpopulation of them (Fig. 1*d*,*e*, Table 2). Indeed, although there are ~25 Gr66a+ neurons per each labellum, we identified an average of five plus or minus two pLB1+ neurons (Thorne et al., 2004; Wang et al., 2004; Dunipace et al., 2001; Tables 1, 2). We confirmed this result by using genetic intersectional strategy between pLB1$^{Gal4}$ and Gr66a$^{LexA}$ (Fig. 3*a*) and by using another driver that broadly targets bitter-sensing gustatory neurons (i.e., Gr32a$^{LexA}$; Fig. 3*c*). Consistently, by using the same strategy and a driver that labels sweet GRNs (Gr5a$^{LexA}$), we did not detect any neurons that are simultaneously pLB1+ and Gr5a+ (Fig. 3*d*). In addition, the expression of the Gal4 inhibitor Gal80 in Gr66a+ neurons (Gr66a$^{LexA}$/LexAop$^{Gal80}$) suppressed the expression of GFP in pLB1+ neurons (pLB1$^{Gal4}$/UAS-mCD8-GFP). No signal was detected in pLB1$^{Gal4}$/UAS-mCD8-GFP flies expressing the Gal80 repressor (Fig. 3*b*). Last, imaging using a panisoform reporter line in which the endogenous PGRP-LB has been GFP tagged at the locus (PGRP-LB::GFP) demonstrated that the endogenous PGRP-LB protein is also produced in Gr66a+ neurons (Fig. 3*e*). Together, these data demonstrate that all the pLB1+ neurons in the proboscis are bitter-sensing neurons.

### Bitter GRNs respond to bacteria and to DAP-type PGN

Because we observed in bitter-sensing gustatory neurons the expression of an enzyme dedicated to the buffering of the NF-κB/IMD response and that the PGN is a proxy to delineate whether bacteria are present, we first tested whether pLB1+ gustatory neurons could be activated by bacterial PGN by performing *in vivo* calcium imaging.

Two types of PGN, which differs for a single amino acid in the stem peptide, are found in bacteria. Whereas the Lysine (Lys)-type PGN is found in Gram-positive bacteria cell wall, the DAP-type PGN forms that of Gram-negative bacteria. Although Lys-type PGN preferentially triggers the *Drosophila* NF-κB/Toll pathway, DAP-type PGN mainly leads to the activation of the NF-κB/IMD pathway (Leulier et al., 2003). Exposing the labella of pLB1$^{Gal4}$/UAS-GCaMP6s flies to DAP-type PGN triggered an increase of the intracellular calcium levels in the SEZ-located axonal projections of labellar pLB1+ neurons, indicating that this subset of gustatory neurons senses and is activated by bacterial DAP-type PGN. Our data demonstrated that pLB1+ neurons responded to DAP-type PGN in a dose-dependent manner and detected caffeine (a bitter compound for flies), but not sucrose, confirming their bitter nature (Fig. 4*a*,*b*, Movies 1, 2).

Considering that the pLB1$^{Gal4}$ transgene drives the expression of Gal4 in neurons other than GRNs and in immune cells, and that all pLB1+ GRNs are GR66a+, we decided to study PGN perception by bitter gustatory neurons in the well-characterized Gr66a+ GRN population. As for labellar pLB1+ gustatory neurons, calcium imaging revealed that DAP-type PGN activates Gr66a+ neurons (Fig. 4*c*,*d*, Movie 3). Together, these results showed that bitter GRNs, some of which express the PGRP-LB protein, are able to respond to DAP-type PGN. Moreover, when we exposed flies to *E. coli*, a Gram-negative bacterium that produces DAP-type PGN and known to activate the NF-κB/IMD cascade in immune tissues, we also detected a response in Gr66a+ neurons, demonstrating that these neurons are able to directly detect bacteria (Fig. 4*c*,*d*). Because of the highly complex biochemical composition of bacteria, we decided to focus the next experiments on the sensing of pure PGN. To evaluate the specificity of this response, pLB1$^{Gal4}$/UAS-GCaMP6s and Gr66a$^{Gal4}$/UAS-GCaMP6s flies were exposed to Lys-type PGN, which does not interact with PGRP-LB and does not activate the NF-κB/IMD cascade (Leulier et al., 2003). When used at concentrations at which DAP-type PGN is active, Lys-type PGN was not able to trigger calcium increase in pLB1+, nor in GR66a+ neurons (Fig. 4*e*,*f*). These data indicate that bitter-sensing gustatory neurons are responsive to the DAP-type PGN found in the cell wall of Gram-negative bacteria.

### Upstream elements of the NF-κB/IMD pathway are required for the response of bitter GRNs to PGN

As some GRNs respond to DAP-type PGN, we tested whether the canonical upstream PGN sensors and downstream NF-κB/IMD pathway components were necessary to transduce its signal, as it is for immune competent cells. For that purpose, *in vivo* calcium imaging experiments in pLB1$^{Gal4}$/UAS-GCaMP6s flies were performed in various NF-κB/IMD mutant background flies. Two PGRP proteins function as upstream DAP-type PGN

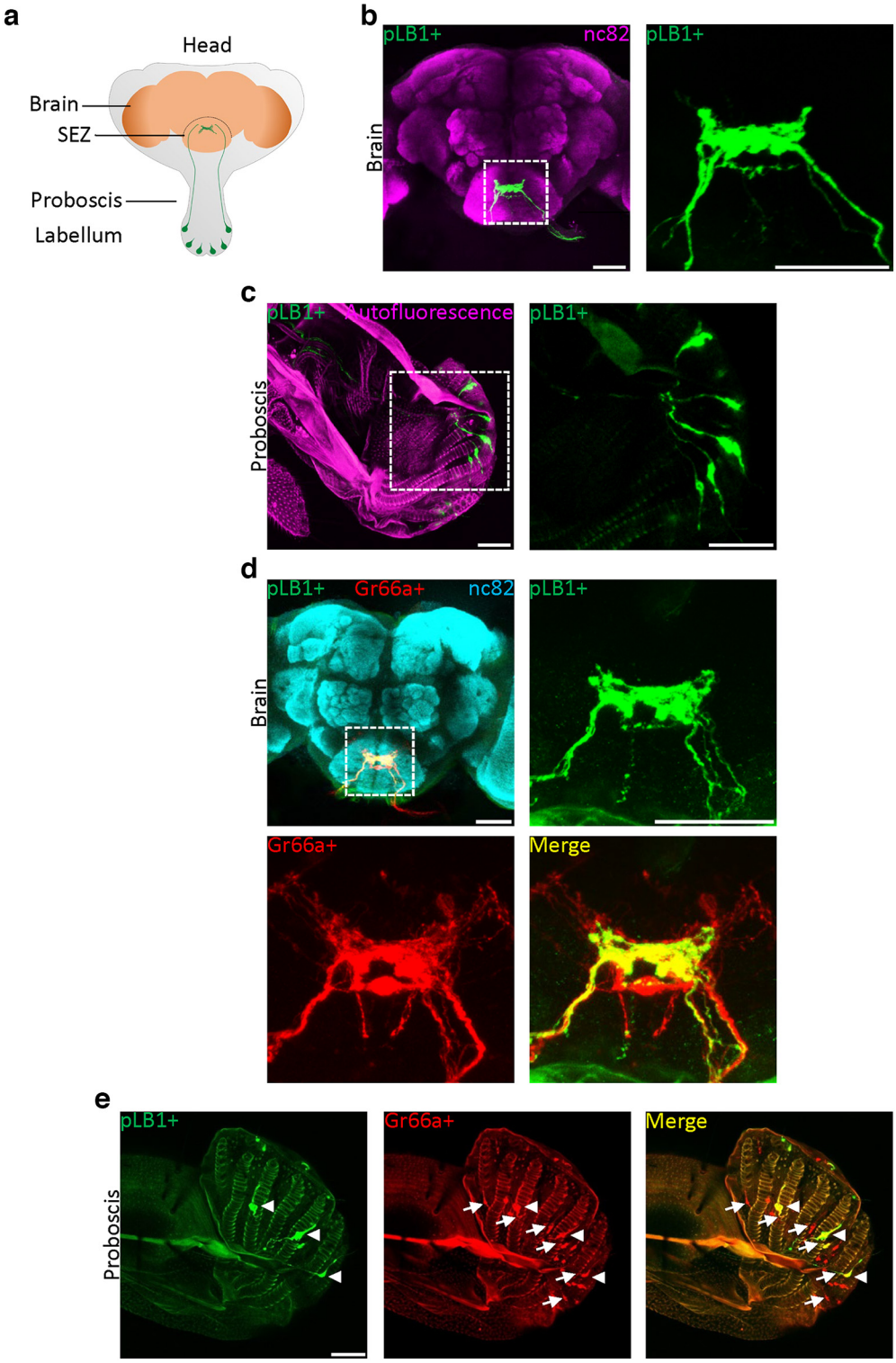


**Figure 1.** An IMD pathway component is expressed in neurons located in the proboscis. Detection of cells expressing pLB1$^{Gal4}$/UAS-mCD8-GFP (pLB1+). ***a***, Schematic representing the fly head and the axonal projections of pLB1+ peripheral neurons (green). The proboscis is an appendix dedicated to the feeding process and hosts neurons dedicated to detection of tastants. The cell bodies of pLB1+ neurons are located in labellar sensilla exposed to the environment and project axons to the brain, specifically in the SEZ. ***b***, In the brain of female flies, labellar pLB1+ neurons project in the SEZ with a reproducible pattern ($n = 25$). Right, Magnification of the SEZ delineated by the white box. ***c***, The projections seen in the SEZ arise from neurons whose cell bodies are located in the tip of the proboscis (Table 1; $n = 32$), the labellum. Right, Magnification of the labellum delineated by the white box. ***d***, ***e***, Immunodetection in the brain (***d***) and detection in the proboscis (***e***) of cells expressing pLB1$^{Gal4}$/UAS-mCD8-GFP (pLB1+) as well as Gr66a-RFP (Gr66a+; $n = 5$ for brains, $n = 6$ for proboscises). ***d***, Top left, Large portion of the brain, Right and bottom, Magnifications of the SEZ delineated by the white box. ***e***, All the pLB1+ projections and neurons (arrowheads) are Gr66a+, whereas not all the Gr66a+ projections and cells (arrows) are pLB1+. Scale bar, 50 $\mu$m. *n*, Number of examined brains or proboscises. Stacks of images were analyzed. For the proboscises, sagittal views, anterior is on the right with dorsal part and maxillary palps sometimes visible at the bottom (Tables 1, 2).

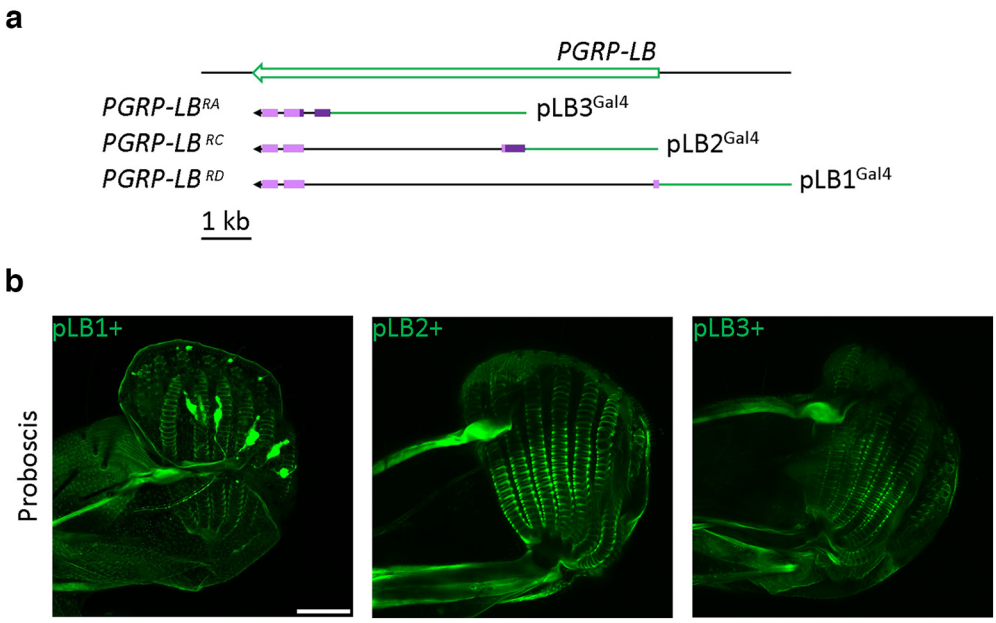


**Figure 2.** pLB2 and pLB3 expressions are not detected in the fly labellum. ***a***, Schematic representation showing the PGRP-LB locus (adapted from FlyBase, http://flybase.org/reports/FBgn0037906.html, and from Kurz et al. (2017). The exonic coding sequences are indicated in light purple, whereas the noncoding exonic sequence is in dark purple. The fragments (green) used to generate the pLB1$^{Gal4}$, pLB2$^{Gal4}$, and pLB3$^{Gal4}$ constructs are indicated (Kurz et al., 2017). ***b***, Detection in the labella of pLB1+ (pLB1$^{Gal4}$/UAS-mCD8-GFP; $n = 32$), pLB2+ (pLB2$^{Gal4}$/UAS-mCD8-GFP; $n = 7$), and pLB3+ (pLB3$^{Gal4}$/UAS-mCD8-GFP; $n = 3$) cells, from left to right, respectively. Stacks of images were analyzed. Scale bar, 50mm. *n*, Number of examined brains or proboscises.

**Table 1. Number of GFP-positive neurons for labellum in pLB1$^{Gal4}$/UAS-mCD8-GFP flies**

| Number of observed pLB1+ neurons (event) | Number of events/total number of proboscises |
|---|---|
| 3 | 5/32 |
| 4 | 6/32 |
| 5 | 11/32 |
| 6 | 6/32 |
| 7 | 3/32 |
| 8 | 1/32 |

The number of times a precise quantity of pLB1+ neurons is detected (event) is shown over the total amount of proboscises observed. Only 1-week-old female flies were analyzed.

**Table 2. Number of cells pLB1+ as well as Gr66a+ in labellum of pLB1$^{Gal4}$, UAS-mCD8-GFP/Gr66a-RFP flies**

| Number of observed pBL1+ neurons | Number of observed Gr66a+ neurons | Number of observed pBL1+/Gr66a+ neurons |
|---|---|---|
| 4 | 19 | 4 |
| 3 | 20 | 3 |
| 3 | 19 | 3 |
| 3 | 17 | 3 |
| 3 | 20 | 3 |
| 4 | 15 | 4 |

The amount of pLB1+ neurons, Gr66a+ neurons and costained cells are presented. Only 1-week-old female flies were analyzed.

(hereafter referred to as PGN) receptors—PGRP-LC and PGRP-LE (Fig. 5*a*). Although caffeine response was unaffected in *PGRP-LC* (*PGRP-LC$^{E12}$*) and *PGRP-LE* (*PGRP-LE$^{112}$*) mutants (Fig. 6*a*), PGN ability to activate pLB1+ neurons was completely abrogated in *PGRP-LC* mutants (Fig. 5*b*), and to a lesser extent, decreased in *PGRP-LE* animals. In contrast, PGN sensing in pLB1+ neurons was not modified in the *PGRP-LB* mutant background compared with control animals (Fig. 5*b*). When we studied the PGN response in Gr66a$^{Gal4}$/UAS-GCamP6s flies, the loss of PGRP-LC was also sufficient to abolish this response, indicating that this membrane-associated receptor is required in bitter-sensing neurons to detect the PGN (Fig. 5*c*).

As previous reports demonstrated that elements of the NF-κB/IMD pathway are expressed and functionally required in some neurons (Kurz et al., 2017; Masuzzo et al., 2019), their implication in mediating the effect of PGN was tested. Although loss-of-function mutants for *Dredd* (*Dredd$^{D55}$*; Fig. 5*a*) were responding normally to caffeine, a strong reduction of calcium signal in pLB1+ neurons was observed in flies stimulated with PGN (Figs. 5*b*,*c*, 6*a*,*c*). The conserved ability of *Dredd* mutants to detect caffeine demonstrated that their unresponsiveness to PGN was neither secondary to neuronal death nor to a loss of cell functionality. To ensure that the NF-κB/IMD pathway was required cell autonomously in gustatory neurons, we used RNAi-mediated cell-specific inactivation. Functional downregulation of the *PGRP-LC*, *IMD*, *Fadd*, and *Dredd* in GR66a+ cells was sufficient to block calcium response after PGN stimulation (Fig. 5*d*). These neurons remained responsive to caffeine (Fig. 6*d*), demonstrating that the inactivation of NF-κB/IMD pathway upstream components specifically impaired the response to PGN. Because most of the reported IMD-dependent responses have been shown to be mediated by the NF-κB transcription factor Relish, we tested its implication in bitter GRNs response to PGN (Myllymaki et al., 2014; Zhai et al., 2018b). Intriguingly, the calcium response of Gr66a+ neurons on proboscis stimulation by PGN or caffeine was not statistically different in Relish RNAi flies compared with wild-type controls (Figs. 5*d*, 6*d*). Altogether, these data demonstrate that Gr66a+ neurons can respond to DAP-type PGN in an IMD-pathway-dependent manner but suggest that it is independent of the canonical Relish transactivator.

### The response of bitter-sensing neurons to peptidoglycan does not require TrpA1 nor Gr66a

A previous work has shown that another ubiquitous component of the Gram-negative bacterial cell wall, LPS, is detected in

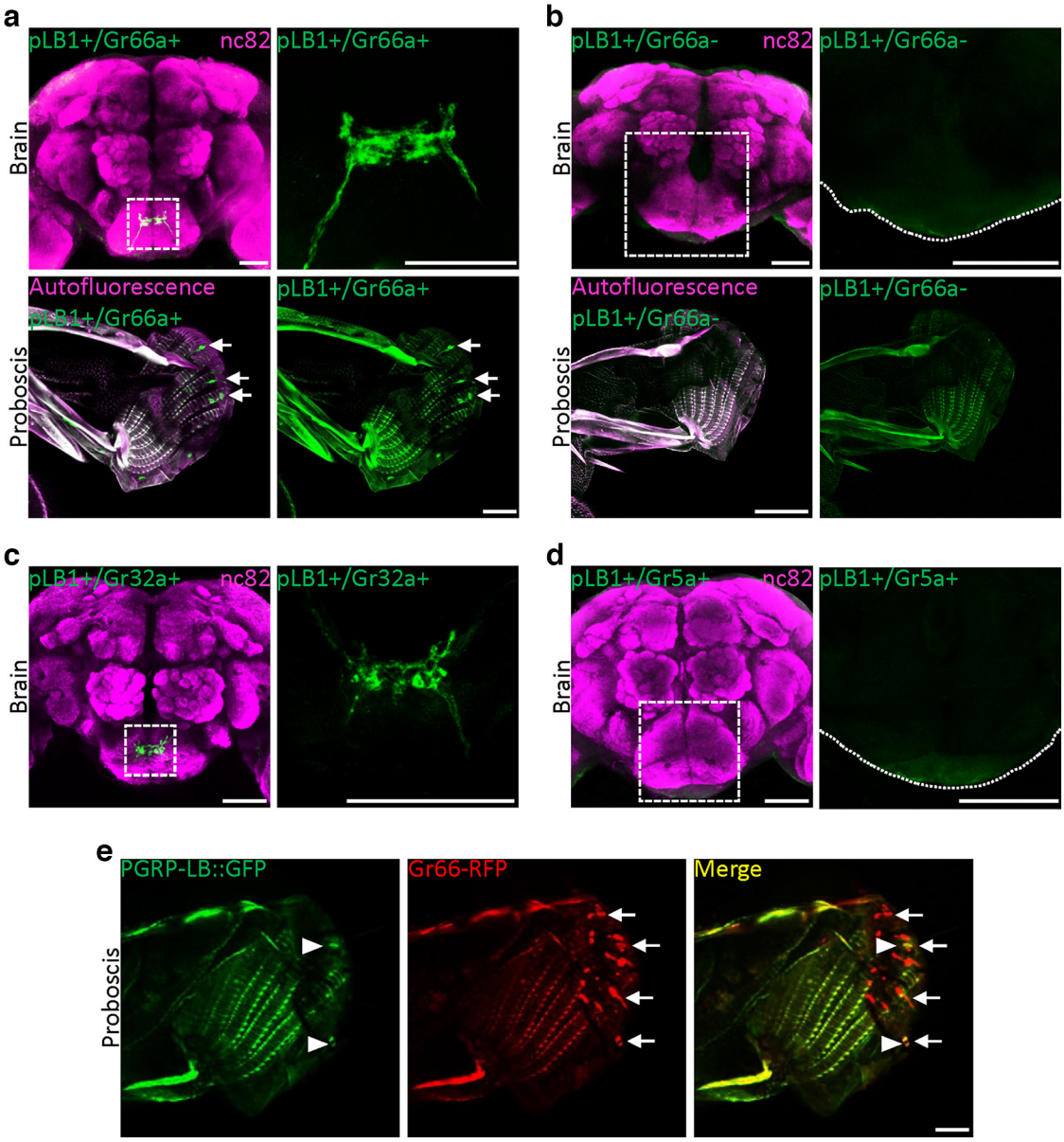


**Figure 3.** pLB1+ neurons in the labellum are exclusively Gr66a+. ***a***, Immunodetection in brain (top) and detection in the proboscis (bottom) of cells pLB1+ as well as Gr66a+ via genetic intersectional strategy (pLB1$^{Gal4}$, Gr66a$^{LexA}$/UAS*frt*STOP*frt*mCD8-GFP, LexAopFLP; $n = 5$ brains, $n = 4$ proboscises). Arrows point to pLB1+/Gr66a+ cellular bodies. ***b***, Immunodetection in brain (top) and detection in the proboscis (bottom) of cells pLB1+ and Gr66a− (pLB1+/Gr66a−) via the expression of the Gal4 inhibitor Gal80 specifically in Gr66a+ cells (pLB1$^{Gal4}$; UAS-mCD8-GFP/Gr66a$^{LexA}$, LexAopGal80; $n = 3$ brains, $n = 4$ proboscises). ***c***, Immunodetection in the brain of cells pLB1+ as well as Gr32a+ via genetic intersectional strategy (pLB1$^{Gal4}$/Gr32a$^{LexA}$; UAS*frt*STOP*frt*mCD8GFP, LexAopFLP; $n = 3$). ***d***, Immunodetection in the brain of cells pLB1+ as well as Gr5a+ via genetic intersectional strategy (pLB1$^{Gal4}$, Gr5a$^{LexA}$/UAS*frt*STOP*frt*mCD8GFP, LexAopFLP; $n = 2$). ***e***, Detection in the proboscis of cells producing the endogenous PGRP-LB (PGRP-LB::GFP) as well as Gr66a-RFP (Gr66a+). All the PGRP-LB::GFP+ cells (arrowheads) are Gr66a+, whereas not all the Gr66a+ cells (arrows) are PGRP-LB::GFP+ ($n = 4$). ***a–d***, Right, Magnifications of the subesophageal zone delineated by the white box. All the images of the proboscis are sagittal views with anterior on the right and dorsal at the bottom. *n*, Number of examined brains or proboscises. Scale bar, 50 $\mu$m.

esophageal Gr66a+ bitter-sensing neurons via the TrpA1 cation channel (Soldano et al., 2016). To assess whether TrpA1 is implicated in the response of neurons to PGN, we performed *in vivo* calcium imaging in *dTrpA*$^{1}$ mutants. The fact that PGN-dependent activation of cells is conserved in *dTrpA*$^{1}$ mutants demonstrated that PGN and LPS are detected by different receptors and certainly trigger different pathways in bitter GRNs (Fig. 6*b*). The non-GPCR gustatory receptor GR66a itself was also not involved in mediating the response to PGN. Altogether, these results suggest that PGRP-LC is the dedicated receptor necessary for PGN detection and transduction in bitter-sensing neurons.

### Activation of the NF-κB/IMD pathway in bitter-sensing neurons modulates aversive behaviors

The ability of PGN to activate calcium release in bitter GRNs prompted us to test whether PGN triggers aversive behaviors in flies. We tested this hypothesis using the FlyPAD device in a two-choice feeding assay (Fig. 7*a*; Itskov et al., 2014). When flies were given a choice between a sucrose-only and a sucrose-plus-PGN solution, no obvious repulsive behavior toward PGN was detected (Figs. 7*b*, 8*a*,*b*). To further evaluate the phenotypical consequences associated with activation of the NF-κB/IMD pathway specifically in the Gr66a+ neurons, we overexpressed the upstream signaling receptor PGRP-LCa in these cells. This

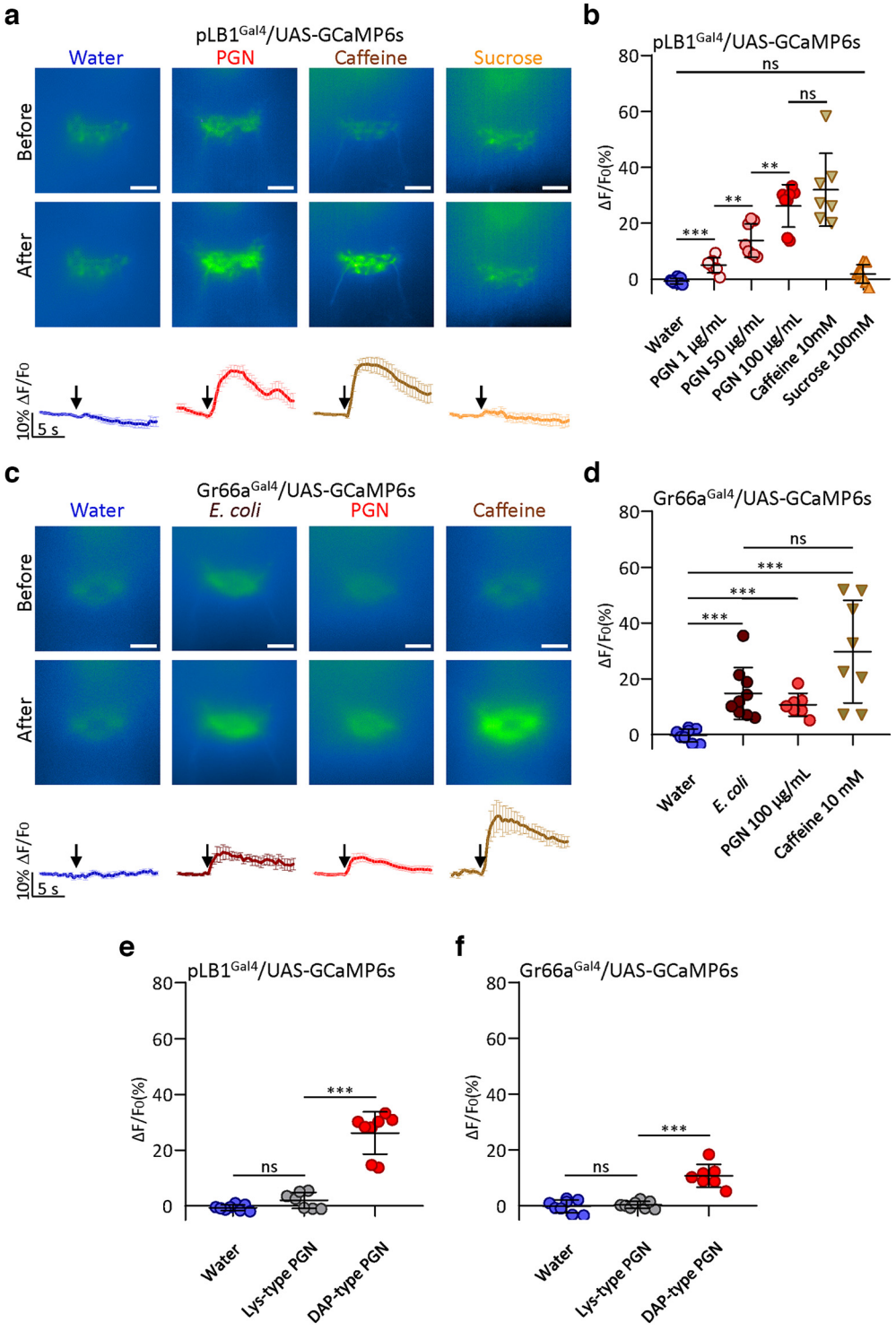


**Figure 4.** Bitter gustatory receptor neurons respond to DAP-type peptidoglycan. ***a–d***, Real-time calcium imaging using the calcium indicator GCaMP6s to assess the *in vivo* neuronal activity in the SEZ of labellar pLB1+ neurons (pLB1$^{Gal4}$/UAS-GCaMP6s; ***a***, ***b***) or bitter gustatory receptor neurons (Gr66a$^{Gal4}$/UAS-GCaMP6s; ***c***, ***d***). ***a***, ***c***, Representative images (top) and averaged fluorescence ± SEM time course of the GCaMP6s intensity variations (ΔF/F0%; bottom). The addition of the chemical on the proboscis at a specific time is indicated by the arrow. ***a***, The images illustrate the GCaMP6s intensity before and after the addition of either water as negative control (left), peptidoglycan (PGN 100 µg/ml; middle), caffeine or sucrose (right) on the proboscis. Scale bar, 20 $\mu$m. ***c***, The images illustrate the GCaMP6s intensity before and after the addition of either water as negative control, *E. coli* K12 (OD600 = 0.5), PGN (100 µg/ml), caffeine, or sucrose (left to right) on the proboscis. Scale bar, 20 $\mu$m. ***b***, Averaged fluorescence intensity of peaks (ΔF/F0) ± SD for water, PGN (different concentrations), caffeine, or sucrose stimulated flies ($n$ = 7–8). Water ($n$ = 8) versus PGN 1 µg/ml ($n$ = 7), $p$ = 0.0006; PGN 1 µg/ml ($n$ = 7) versus PGN 50 µg/ml ($n$ = 8), $p$ = 0.0022; PGN 50 µg/ml ($n$ = 8) versus PGN 100 µg/ml ($n$ = 8), $p$ = 0.0047; caffeine 10 mM ($n$ = 7) versus PGN 100 µg/ml ($n$ = 8), $p$ = 0.6943; sucrose 100 mM ($n$ = 8) versus water ($n$ = 8), $p$ = 0.083; nonparametric $t$ test, two tailed Mann–Whitney test. ***d***, Averaged fluorescence intensity of peaks ± SD for water, *E. coli* K12(OD600 = 0.5), PGN (100 µg/ml), caffeine, or sucrose stimulated flies ($n$ = 7–9). Water ($n$ = 8) versus *E. coli* ($n$ = 9), $p < 0.0001$; PGN 100 µg/ml ($n$ = 7) versus water ($n$ = 8), $p$ = 0.0003; caffeine 10 mM ($n$ = 8) versus water ($n$ = 8), $p$ = 0.0003; *E. coli* ($n$ = 9) versus PGN 100 µg/ml ($n$ = 7), $p$ = 0.536; *E. coli* ($n$ = 9) versus caffeine 10 mM ($n$ = 8), $p$ = 0.0927; caffeine 10 mM ($n$ = 8) versus PGN 100 µg/ml ($n$ = 7), $p$ = 0.0721; nonparametric $t$ test, two tailed Mann–Whitney test. ***e***, Averaged fluorescence intensity of peaks (ΔF/F0) ± SD for pLB1$^{Gal4}$/UAS-GCaMP6s ($n$ = 7–8) flies exposed to water, Lys-type PGN (100 µg/ml) or DAP-type PGN (100 µg/ml). Water ($n$ = 8) versus Lys-type PGN ($n$ = 7), $p$ = 0.1206; water ($n$ = 8) versus DAP-type PGN 100 µg/ml ($n$ = 8), $p$ = 0.0002; DAP-type PGN 100 µg/ml ($n$ = 8) versus Lys-type PGN 100 µg/ml ($n$ = 7), $p$ =

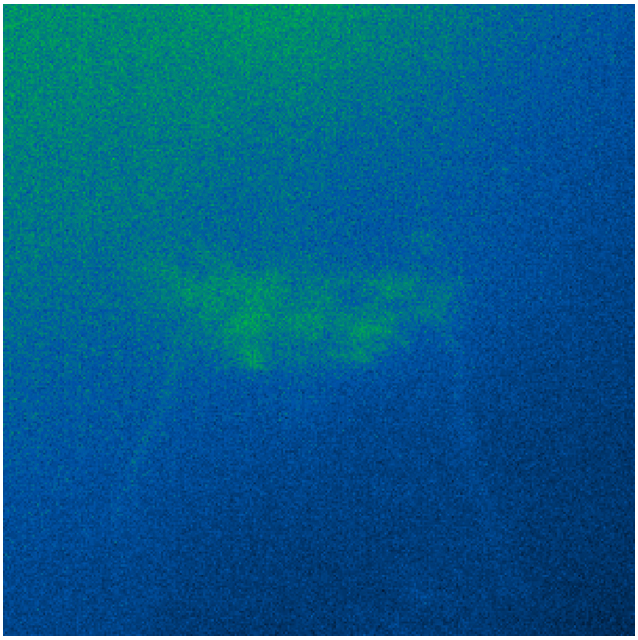

**Movie 1.** pLB1+ neurons respond *in vivo* to PGN. Real-time calcium imaging using the calcium indicator GCaMP6s to assess the *in vivo* neuronal activity in the subesophageal zone of pLB1 neurons (pLB1$^{Gal4}$/UAS-GCaMP6s). Effect of peptidoglycan solution stimulation (100 μg/ml) on the proboscis. GFP signal was recorded every 500 ms, and the PGN was added 1 s after the beginning of the recording. [View online]

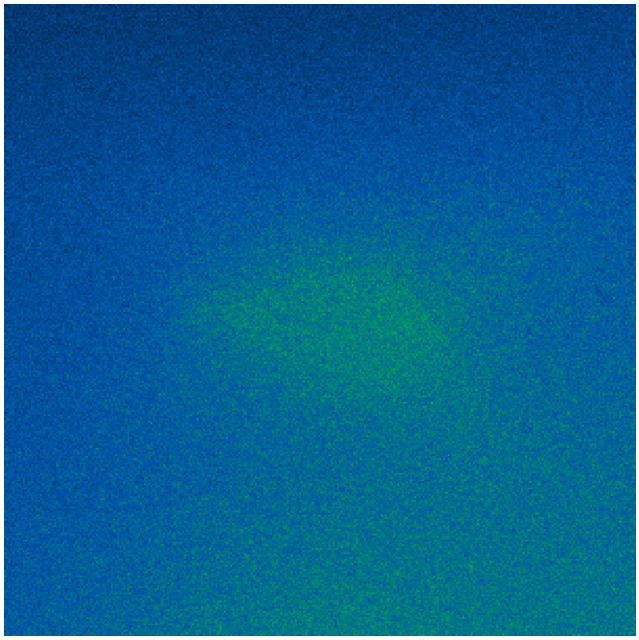

**Movie 2.** pLB1+ neurons respond *in* vivo to caffeine. Real-time calcium imaging using the calcium indicator GCaMP6s to assess the *in vivo* neuronal activity in the subesophageal zone of pLB1 neurons (pLB1$^{Gal4}$/UAS-GcaMP6s). Effect of caffeine solution stimulation (10 mM) on the proboscis. GFP signal was recorded every 500 ms, and the caffeine was added 1 s after the beginning of the recording. [View online]

ectopic expression may hypersensitize the cells to PGN and has been shown to induce forced dimer receptor formation and hence trigger downstream signaling in the absence of the ligand or with lower amounts of it. In a two-choice feeding assay, flies in which PGRP-LCa was overexpressed in GR66a+ neurons showed an increased repulsion toward the solution containing PGN (Fig. 7*c*). This behavior, which was not observed in control animals, was abolished by the simultaneous knockdown of the NF-κB/IMD downstream element *Fadd* (Fig. 7*d*). Thus, when sensitized following overexpression of the PGRP-LCa receptor, flies can discriminate, via the IMD pathway, between a sucrose containing PGN solution and a sucrose-only solution. Because lactic acid bacteria *Enterococci* are critical modulators to attract *Drosophila* to lay eggs on decaying food (Liu et al., 2017), we then tested whether IMD-dependent activation of bitter-sensing neurons would have an impact on egg-laying site preference. Although we were unable to detect any bias of egg laying toward PGN contaminated media (data not shown), we observed that PGRP-LCa overexpression in Gr66a+ neurons directly led to a decreased oviposition (Fig. 7*e*,*f*). This decreased egg laying when PGRP-LCa is expressed in bitter-sensing gustatory neurons was confirmed using Gr32a$^{Gal4}$ as another bitter GRNs driver (Fig. 8*c*). These results suggesting that NF-κB/IMD pathway

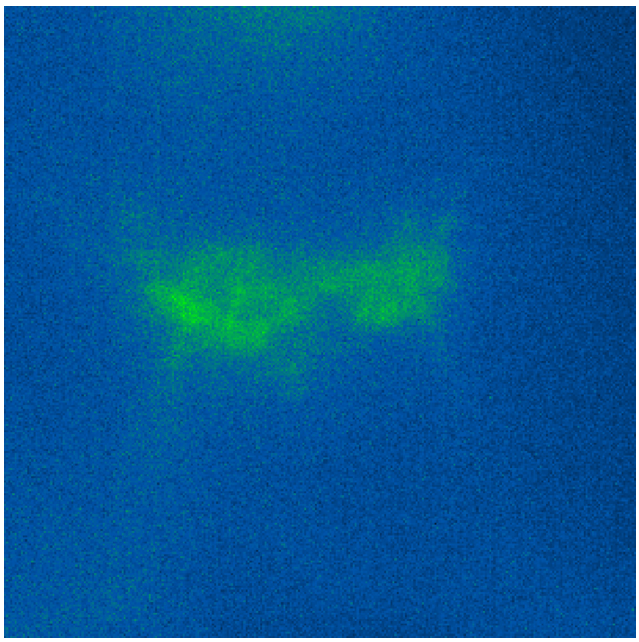

**Movie 3.** Gr66a+ neurons respond *in vivo* to PGN. Real-time calcium imaging using the calcium indicator GCaMP6s to assess the *in vivo* neuronal activity in the subesophageal zone of bitter-sensing neurons (Gr66a$^{Gal4}$/UAS-GCaMP6s). Effect of peptidoglycan solution stimulation (100 μg/ml). GFP signal was recorded every 500 ms, and the PGN was added 1 s after the beginning of the recording. [View online]

activation in bitter GRNs reduces female egg laying were further confirmed by showing that this effect could be suppressed by the simultaneous RNAi-mediated *Fadd* inactivation in Gr66a+ neurons (Fig. 7*g*). In contrast, simultaneous knockdown of the transcription factor *Relish* did not have an impact on the egg-laying decrease, indicating that this transactivator is not required for

←

0.0003; nonparametric *t* test, two-tailed Mann–Whitney test. ***f***, Averaged fluorescence intensity of peaks (ΔF/F0) ± SD for Gr66a$^{Gal4}$/UAS-GCaMP6s ($n$ = 7–8) flies exposed to water, Lys-type PGN (100 μg/ml) or DAP-type PGN (100 μg/ml). Water ($n$ = 8) versus Lys-type PGN ($n$ = 8), $p$ = 0.7984; water ($n$ = 8) versus DAP-type PGN 100 μg/ml ($n$ = 7), $p$ = 0.0003; DAP-type PGN 100 μg/ml ($n$ = 7) versus Lys-type PGN 100 μg/ml ($n$ = 8), $p$ = 0.0003; nonparametric *t* test, two-tailed Mann–Whitney test. *n*, Number of analyzed animals (single dots in graphs) for each condition; ns, not significant. $p \geq 0.05$, *$0.05 \geq p > 0.01$, ns; **$0.01 \geq p \geq 0.001$, ***$p < 0.001$; some data did not pass the D'Agostino–Pearson normality test; nonparametric tests were performed.

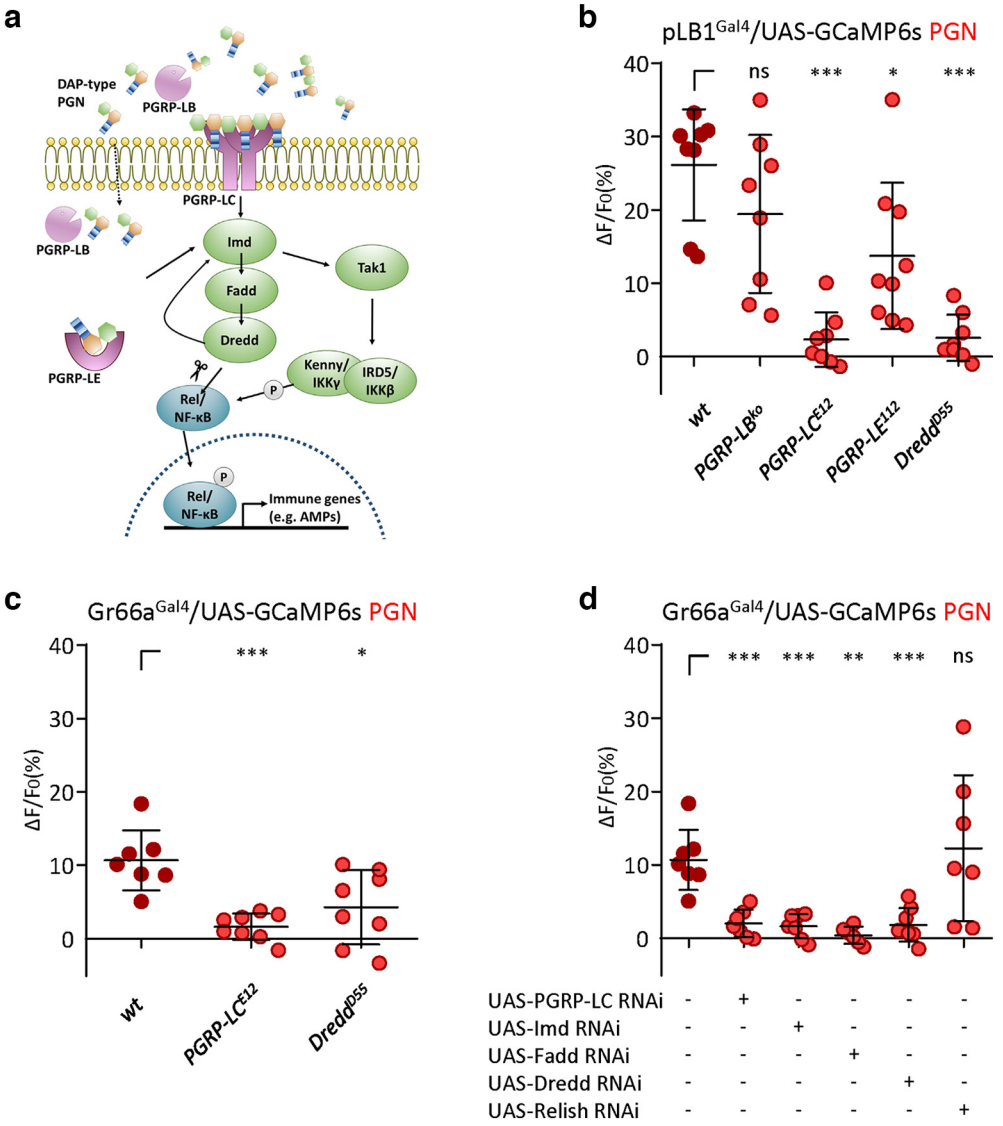


**Figure 5.** The PGN detection in pLB1+ and Gr66a+ neurons require upstream elements of the NF-κB/IMD pathway. ***a***, Schematic of the canonical NF-κB/IMD pathway in *Drosophila*. ***b–d***, Real-time calcium imaging using the calcium indicator GCaMP6s to assess the *in vivo* neuronal activity in the SEZ of labellar pLB1+ neurons (pLB1$^{Gal4}$/UAS-GCaMP6s; ***b***) or bitter gustatory receptor neurons (Gr66a$^{Gal4}$/UAS-GCaMP6s; ***c***, ***d***). ***b***, Averaged fluorescence intensity of peaks (ΔF/F0) ± SD for pLB1$^{Gal4}$/UAS-GCaMP6s ($n = 8–9$) flies in different mutant backgrounds and exposed to PGN (100 μg/ml). *PGRP-LB$^{ko}$* ($n = 8$) versus *WT* ($n = 8$), $p = 0.1605$; *PGRP-LC$^{E12}$* ($n = 8$) versus *WT* ($n = 8$), $p = 0.0002$; *PGRP-LE$^{112}$* ($n = 9$) versus *WT* ($n = 8$), $p = 0.0206$; *Dredd$^{D55}$* ($n = 8$) versus *WT* ($n = 8$), $p = 0.0002$; nonparametric *t* test, two-tailed Mann–Whitney test. ***c***, Averaged fluorescence intensity of peaks (ΔF/F0) ± SD for Gr66a$^{Gal4}$/UAS-GCaMP6s ($n = 7–8$) flies in different mutant backgrounds and exposed to PGN (100 μg/ml). *PGRP-LC$^{E12}$* ($n = 8$) versus *WT* ($n = 7$), $p = 0.0003$; *Dredd$^{D55}$* ($n = 8$) versus *WT* ($n = 7$), $p = 0.0205$; nonparametric *t* test, two-tailed Mann–Whitney test. ***d***, Averaged fluorescence intensity of peaks (ΔF/F0) ± SD for Gr66a$^{Gal4}$/UAS-GCaMP6s animals expressing RNAi targeting different elements of the NF-κB/IMD pathway and exposed to PGN (100 μg/ml; $n = 6–8$). PGRP-LC RNAi ($n = 7$) versus control (Ctrl; $n = 7$), $p = 0.0006$; Imd RNAi ($n = 7$) versus Ctrl ($n = 7$), $p = 0.0006$; Fadd RNAi ($n = 6$) versus Ctrl ($n = 7$), $p = 0.0012$; Dredd RNAi ($n = 8$) versus Ctrl ($n = 7$), $p = 0.0006$; Relish RNAi ($n = 7$) versus Ctrl ($n = 7$), $p = 0.9015$; nonparametric *t* test, two-tailed Mann–Whitney test. *n*, Number of analyzed animals (single dots in graphs) for each condition; ns, not significant. $p \geq 0.05$, ns; *$0.05 \geq p > 0.01$; **$0.01 \geq p \geq 0.001$; ***$p < 0.001$; some data did not pass the D'Agostino–Pearson normality test, nonparametric tests were performed.

this PGN-mediated behavioral response (Fig. 7*g*). We previously showed that PGN-dependent NF-κB/IMD pathway activation in a subset of brain octopaminergic neurons was sufficient to reduce female egg laying, a phenomenon reproduced with Kir2.1 overexpression in these neurons, suggesting the PGN-dependent inactivation of this octopaminergic neurons (Masuzzo et al., 2019). Importantly, inactivating the Gr66a+ cells via Kir2.1 expression did not phenocopy the egg-laying drop caused by inactivation of octopaminergic neurons, suggesting that PGRP-LCa overexpression triggered activation of Gr66a+ neurons instead (Fig. 8*d*). Consistently, conditional Gr66a+ cells activation via TrpA1 overexpression, which leads to inward current flux of cations, decreased female egg laying (Fig. 7*h*). Together, these data demonstrate that receptor and transducers of the NF-κB/IMD pathway (but not the downstream NF-κB transcription factor Relish) are expressed and functionally required in bitter-sensing-neurons to mediate a behavioral response toward PGN.

## Discussion

This study demonstrates that some neurons of the gustatory system detect peptidoglycan, one of the main conserved and ubiquitous cell-wall bacterial components. In bitter-sensing gustatory neurons, this detection is mainly mediated by the IMD pathway PGRP-LC receptor and thus probably not by classical Gr proteins such as Gr66a. The PGN signal is transduced by the known

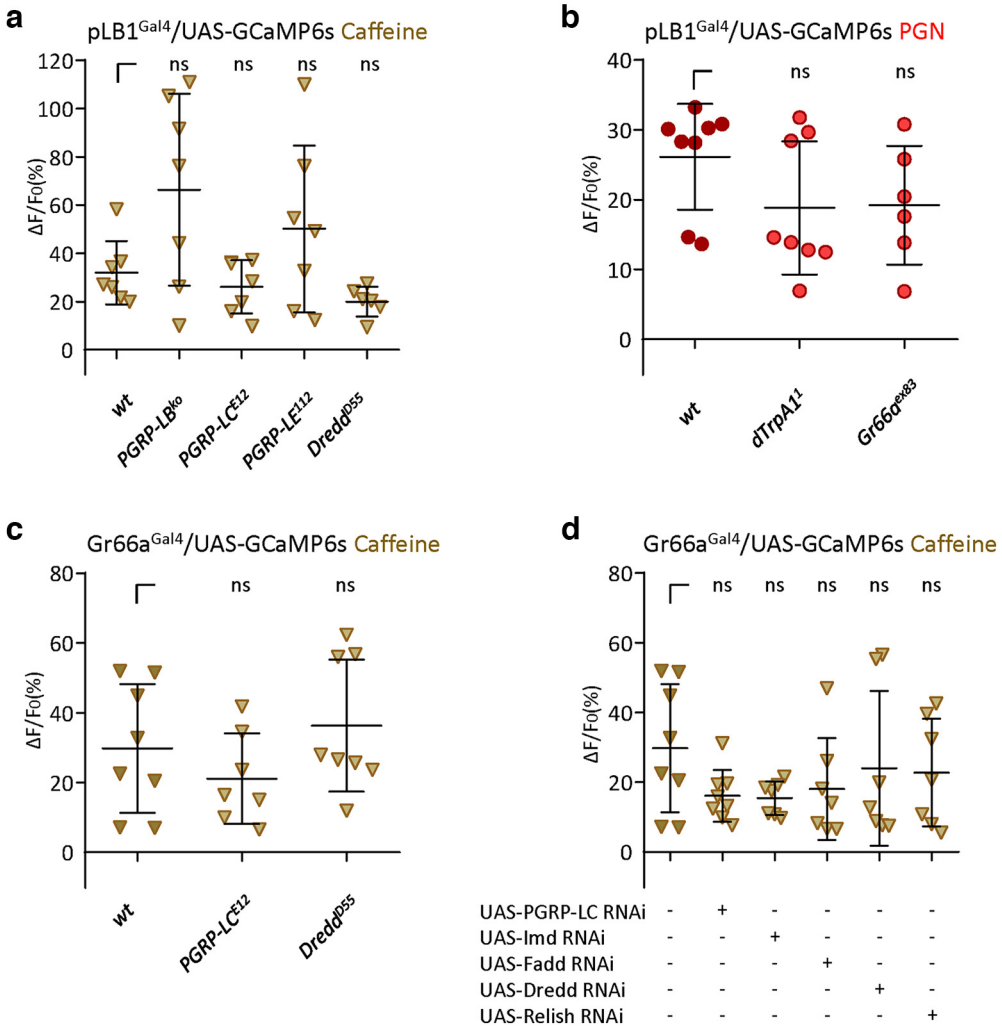


**Figure 6.** The NF-κB/IMD pathway is not required for bitter-sensing gustatory neurons response to caffeine and pLB1+ neurons response to PGN does not necessitate Gr66a or dTrpA1. ***a–d***, Real-time calcium imaging using the calcium indicator GCaMP6s to assess the *in vivo* neuronal activity in the SEZ of pLB1+ (***a***, ***b***) or Gr66a+ (***c***, ***d***) neurons. ***a***, Averaged fluorescence intensity of peaks (ΔF/F0) ± SD for pLB1$^{Gal4}$/UAS-GCaMP6s ($n$ = 6–7) flies in different mutant backgrounds exposed to caffeine (10 mM). *PGRP-LB$^{ko}$* ($n$ = 7) versus *WT* ($n$ = 7), $p$ = 0.1282; *PGRP-LC$^{E12}$* ($n$ = 7) versus *WT* ($n$ = 7), $p$ = 0.62; *PGRP-LE$^{112}$* ($n$ = 7) versus *WT* ($n$ = 7), $p$ = 0.535; *Dredd$^{D55}$* ($n$ = 6) versus *WT* ($n$ = 7), $p$ = 0.0734; nonparametric *t* test, two-tailed Mann–Whitney test. ***c***, Averaged fluorescence intensity of peaks (ΔF/F0) ± SD for Gr66a$^{Gal4}$/UAS-GCaMP6s ($n$ = 7–8) flies in different mutant backgrounds exposed to caffeine (10 mM). *PGRP-LC$^{E12}$* ($n$ = 7) versus *WT* ($n$ = 8), $p$ = 0.3969; *Dredd$^{D55}$* ($n$ = 8) versus *WT* ($n$ = 8), $p$ = 0.3282; nonparametric *t* test, two-tailed Mann–Whitney test. ***b***, Averaged fluorescence intensity of peaks ± SD for pLB1$^{Gal4}$/UAS-GCaMP6s flies in different mutant backgrounds exposed to peptidoglycan (100 μg/ml; $n$ = 6-8). *dTrpA1$^{1}$* ($n$ = 8) versus *WT* ($n$ = 8), $p$ = 0.1304; Gr66$^{ex83}$ ($n$ = 6) versus *WT* ($n$ = 8), $p$ = 0.1812; nonparametric *t* test, two-tailed Mann–Whitney test. ***d***, Averaged fluorescence intensity of peaks ± SD for Gr66a$^{Gal4}$/UAS-GCaMP6s animals expressing RNAi against IMD pathway elements and exposed to caffeine (10 mM; $n$ = 7–8). PGRP-LC RNAi ($n$ = 8) versus control (Ctrl; $n$ = 8), $p$ = 0.1605; Imd RNAi ($n$ = 7) versus Ctrl ($n$ = 8), $p$ = 0.152; Fadd RNAi ($n$ = 7) versus Ctrl ($n$ = 8), $p$ = 0.1893; Dredd RNAi ($n$ = 7) versus Ctrl ($n$ = 8), $p$ = 0.8665; Relish RNAi ($n$ = 7) versus Ctrl ($n$ = 8), $p$ = 0.4634; nonparametric *t* test, two-tailed Mann–Whitney test. $n$, Number of analyzed animals (single dots in graphs) for each condition; ns, not significant. $p \geq 0.05$, ns; *$0.05 \geq p > 0.01$; **$0.01 \geq p \geq 0.001$; ***$p < 0.001$; some data did not pass the D'Agostino–Pearson normality test, nonparametric tests were performed.

cytosolic members of the IMD pathway such as Fadd and Dredd. Together with previous reports, these results confirm the key role played by the PGRP/IMD module in regulating many of the interactions between PGN and flies. This specific recognition step, which takes place at the cell membrane via PGRP-LC or within the cells via PGRP-LE, has been shown to control the production of antibacterial effectors by immune-competent cells, to alter the egg-laying rate of infected females, and to allow the physiological adaptation of the flies to their infectious status (Hedengren et al., 1999; Guo et al., 2014; Kurz et al., 2017; Charroux et al., 2018; Zhai et al., 2018a; Masuzzo et al., 2019; Kobler et al., 2020). Interestingly, although the initial MAMP/PRR recognition event is conserved among these processes, the downstream molecular mechanisms that transduce the signal are context dependent. While both the PGN-dependent activation of an immune response in adipocytes, hemocytes, or enterocytes, and the inhibition of VUM III octopaminergic brain neurons rely on the nuclear NF-κB/Relish protein, the transcriptionally regulated effectors are likely to be different (Buchon et al., 2014; Masuzzo et al., 2019). The response of bitter-sensing-neurons to PGN depends on a noncanonical IMD pathway in which NF-κB/Relish is not required. Interestingly, PGRP-LC and some downstream IMD components are also required at the presynaptic terminal of *Drosophila* motoneurons for robust presynaptic homeostatic plasticity (Harris et al., 2015, 2018). The local modulation of the presynaptic vesicle release, which occurs in seconds following inhibition of postsynaptic glutamate receptors, required PGRP-LC, Tak1 but is also Relish independent. These data and ours raise important questions regarding how the activation of the upstream elements of the

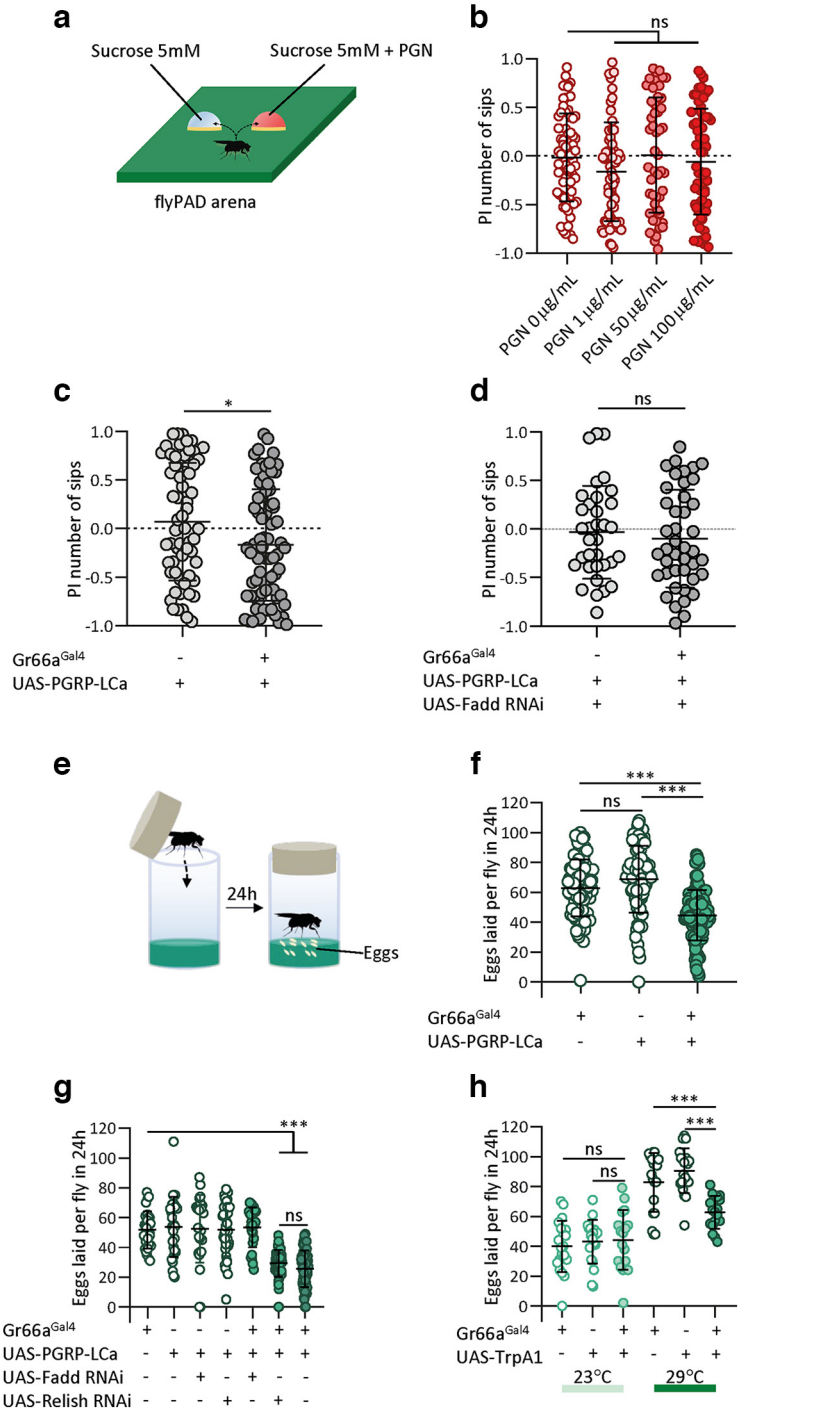


**Figure 7.** Overexpression of the PGN receptor PGRP-LCa in bitter-sensing neurons modulates feeding preference toward peptidoglycan and oviposition behavior. ***a***, Schematic of the two-choice feeding assay using the flyPAD device (Itskov et al., 2014). Individual flies are given the choice between a sucrose solution (5 mM) and a sucrose solution (5 mM) plus PGN and tested for 1 h. ***b–d***, Feeding preference is expressed as a Preference Index (PI) based on the number of sips (see above, Materials and Methods). ***b***, Feeding preference of wild-type (*Canton S*) flies exposed to two sucrose solutions (5 mM), one of which contains PGN (different concentrations are tested and indicated in the *x*-axis; $n = 50–68$). Control ($n = 68$) versus PGN 1 µg/ml ($n = 63$), $p = 0.0757$; control ($n = 68$) versus PGN 50 µg/ml ($n = 50$), $p = 0.8558$; control ($n = 68$) versus PGN 100 µg/ml ($n = 64$), $p = 0.5605$; nonparametric *t* test, two-tailed Mann–Whitney test. ***c***, Feeding preference of flies overexpressing PGRP-LCa in bitter taste neurons ($Gr66a^{Gal4}$/UAS-PGRP-LCa) and controls exposed to two sucrose solutions (5 mM), one of which contains PGN (100 µg/ml; $n = 61–73$). Control ($n = 61$) versus $Gr66a^{Gal4}$/UAS-PGRP-LCa ($n = 73$), $p = 0.0198$; nonparametric *t* test, two-tailed Mann–Whitney test. ***d***, Feeding preference of flies overexpressing simultaneously PGRP-LCa and UAS-Fadd RNAi in bitter taste neurons ($Gr66a^{Gal4}$/UAS-PGRP-LCa, UAS-Fadd RNAi) and control animals exposed to two sucrose solutions (5 mM), one of which contains PGN (100 µg/ml; $n = 49–52$). Control ($n = 34$) versus $Gr66a^{Gal4}$/UAS-Fadd RNAi, UAS-PGRP-LCa ($n = 42$), $p = 0.5712$; nonparametric *t* test, two-tailed Mann–Whitney test. ***e***, Schematic of the oviposition assay. Individual flies are transferred to fresh tubes and allowed to lay eggs for 24 h. ***f***, Eggs laid per 24 h by flies overexpressing PGRP-LCa in bitter taste neurons ($Gr66a^{Gal4}$/UAS-PGRP-LCa) and control animals ($n = 80–92$). $Gr66a^{Gal4}/+$ ($n = 90$) versus UAS-PGRP-LCa/+ ($n = 80$), $p = 0.1265$; $Gr66a^{Gal4}$/UAS-PGRP-LCa ($n = 92$) versus UAS-PGRP-LCa/+ ($n = 80$), $p \leq 0.0001$; $Gr66a^{Gal4}$/UAS-PGRP-LCa ($n = 92$) versus $Gr66a^{Gal4}/+$ ($n = 90$), $p \leq 0.0001$; nonparametric ANOVA test, Dunn's multiple-comparison test. ***g***, Eggs laid per 24 h by flies overexpressing simultaneously PGRP-LCa and Fadd RNAi or Relish RNAi in bitter-sensing gustatory neurons ($Gr66^{Gal4}$/UAS-PGRP-LCa, UAS-Fadd RNAi) and control animals ($n = 24–76$). Detailed statistical analyses and population sizes for this experiment can be found at https://figshare.com/articles/online_resource/Raw_data_and_statistics_for_each_figure_xlsx/20160395; nonparametric ANOVA test, Dunn's multiple-comparison test. ***h***, Eggs laid per 24 h by flies overexpressing TrpA1 in bitter-sensing neurons ($Gr66^{Gal4}$/UAS-$TrpA^1$) and control animals, at a permissive (23°C) and restrictive (29°C) temperature ($n = 18–20$). $Gr66a^{Gal4}/+$ 23°C ($n = 20$) versus $Gr66a^{Gal4}$/UAS-TrpA1 23°C ($n = 20$), $p > 0.9999$; $Gr66a^{Gal4}$/UAS-TrpA1 23°C ($n = 20$) versus +/UAS-TrpA1 23°C ($n = 20$), $p > 0.9999$; $Gr66a^{Gal4}/+$ 29°C ($n = 19$) versus $Gr66a^{Gal4}$/UAS-TrpA1 29°C ($n = 20$), $p = 0.0031$; $Gr66a^{Gal4}$/UAS-TrpA1 29°C ($n = 20$) versus +/UAS-TrpA1 29°C (n = 19), $p < 0.0001$; nonparametric ANOVA test, Dunn's multiple-comparison test. Average PI ± SD of at least three independent trials (***b–d***). *$0.05 > p > 0.01$; $p > 0.05$, not significant (ns); nonparametric *t* test, Mann–Whitney test. Average numbers of eggs laid per fly per 24 h ± SD from at least two independent trials with at least 19 females per trial, genotype and condition used (***f–h***). $p \geq 0.05$, not significant (ns); * $0.05 \geq p > 0.01$; **$0.01 \geq p \geq 0.001$; ***$p < 0.001$; some data did not pass the D'Agostino–Pearson normality test, nonparametric tests were performed, nonparametric ANOVA, Dunn's multiple-comparison test. *n*, Number of analyzed animals (single dots in graphs) for each condition.

IMD cascade is modifying neuronal activity, a topic for future studies. Previous biochemical studies have shown that IMD signaling is rapid, occurring in seconds, a time frame consistent with its role at the synapse and now in bitter-sensing neurons signal transduction (Stoven et al., 2000). Another possibility for the involvement of the IMD pathway in the bitter-sensing neurons would be that the expression of a yet to be identified PGN sensor requires the PGRP/IMD module for a permissive signal on stimulation by environmental bacteria.

Our data show that flies can perceive PGN, a component of the bacteria cell wall, via bitter-sensing neurons. These findings are complementary to observations made for another cell wall component in Gram-negative bacteria, called LPS, which triggers feeding and oviposition avoidance in *Drosophila* through the activation of bitter-sensing neurons (Soldano et al., 2016). Although LPS induced-avoidance behavior is mediated through the canonical chemosensory

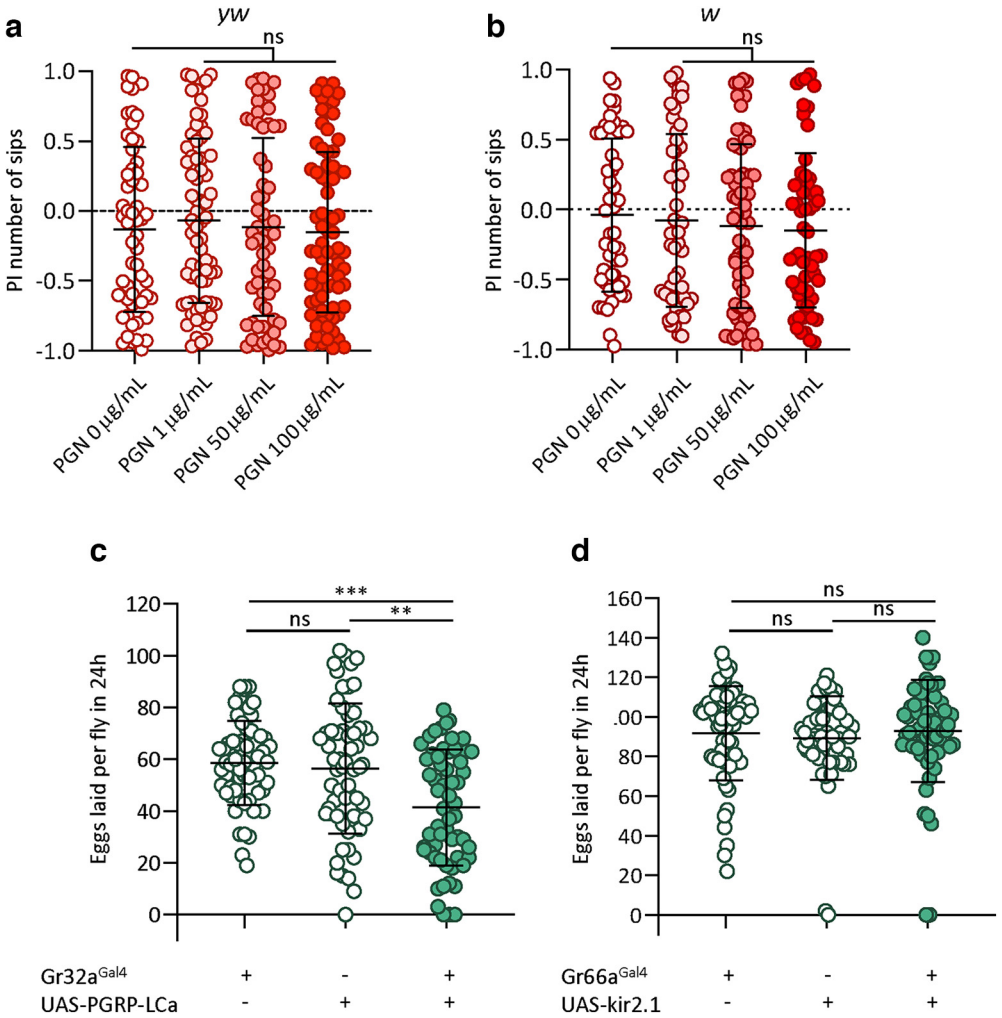


**Figure 8.** Although PGN is neither attractive nor aversive for wild-type flies in two-choice feeding assay, IMD pathway activation in bitter-sensing neurons inhibits egg laying. ***a***, Flies exposed to two sucrose solutions (5 mM), one of which contains PGN (different concentrations are tested and indicated in the *x*-axis), feeding preference of *yw* ($n = 58$–77). Control ($n = 58$) versus PGN 1 µg/ml ($n = 71$), $p = 0.5411$; control ($n = 58$) versus PGN 50 µg/ml ($n = 63$), $p = 0.9732$; control ($n = 58$) versus PGN 100 µg/ml ($n = 77$), $p = 0.8681$; nonparametric *t* test, two tailed Mann–Whitney test. ***b***, Flies exposed to two sucrose solutions (5 mM), one of which contains PGN (different concentrations are tested and indicated in the *x*-axis), feeding preference of *w* ($n = 50$–63) flies exposed to two sucrose solutions (5 mM). Control ($n = 50$) versus PGN 1 µg/ml ($n = 52$), $p = 0.5596$; control ($n = 50$) versus PGN 50 µg/ml ($n = 63$), $p = 0.3945$; control ($n = 50$) versus PGN 100 µg/ml ($n = 58$), $p = 0.3034$; nonparametric *t* test, two tailed Mann–Whitney test. ***c***, Eggs laid per 24 h (24 h) by flies overexpressing PGRP-LCa in bitter-sensing gustatory neurons ($Gr32a^{Gal4}$/UAS-PGRP-LCa) and control animals ($n = 60$). Gr32a Gal4/+ ($n = 60$) versus $Gr32a^{Gal4}$/UAS-PGRP-LCa ($n = 60$), $p = 0.0005$; UAS-PGRP-LCa/+ ($n = 60$) versus $Gr32a^{Gal4}$/UAS-PGRP-LCa ($n = 60$), $p = 0.0034$; $Gr32a^{Gal4}$/+ ($n = 60$) versus +/UAS-PGRP-LCa ($n = 60$), $p > 0.9999$; nonparametric ANOVA test, Dunn's multiple-comparison test. ***d***, Eggs laid per 24 h by flies overexpressing kir2.1 in bitter taste neurons ($G66a^{Gal4}$/UAS-kir2.1) and control animals ($n = 60$). $Gr66a^{Gal4}$/+ ($n = 60$) versus $Gr66a^{Gal4}$/UAS-kir2.1 ($n = 60$), $p > 0.9999$; UAS-kir2.1/+ ($n = 60$) versus $Gr66a^{Gal4}$/UAS-kir2.1 ($n = 60$), $p = 0.5258$; $Gr66a^{Gal4}$/+ ($n = 60$) versus +/UAS-kir2.1 ($n = 60$), $p = 0.8145$; nonparametric ANOVA test, Dunn's multiple-comparison test. ***a***, ***b***, Shown are the average Preference Index (PI) ± SD of at least five independent trials. ***$p < 0.0001$; $p > 0.05$, not significant (ns); nonparametric *t* test, Mann–Whitney test. ***c***, ***d***, Shown are the average numbers of eggs laid per fly per 24 h ± SD from at least two independent trials with at least 20 females per trial, genotype, and condition used. $p \geq 0.05$, ns; *$0.05 \geq p > 0.01$; **$0.01 \geq p \geq 0.001$; ***$p < 0.001$; some data did not pass the D'Agostino–Pearson normality test, nonparametric tests were performed, nonparametric ANOVA, Dunn's multiple-comparison test. *n*, Number of analyzed animals (single dots in graphs) for each condition.

cation channel TrpA1, we show that PGN-induced activation of bitter-sensing neurons seems to be independent of it. It seems to be also independent of the classical Gr receptors but depend on a dedicated PGN sensor used in other contexts. We demonstrate that the bitter response on PGN stimulation is dependent on the IMD pathway, which not only regulates a feeding aversion for PGN but also modulate oviposition rate. This indicates that PGN detection by gustatory neurons and its relay by the IMD pathway is probably an informative environmental cue for flies. Our approach focusing on purified PGN allows us to directly link a molecule to the neurons and the proteins that perceive it. However, the behavior of flies in a natural environment most probably corresponds to a highly complex integration of multiple intricate signals perceived by different sensory systems of the animal. For instance, lactic acid, which is produced by some bacteria is also sensed by gustatory neurons (Stanley et al., 2021). In this respect, it remains difficult to appreciate which concentrations of bacteria-derived products animal sensory system are exposed to in their natural environment. Assays estimated the amount of LPS at the surface of fruits of ~1000 µg/ml (Soldano et al., 2016). To our knowledge, no such studies were performed for PGN. It should also be mentioned that the amount of PGN released by bacteria is highly dependent on the species considered and the bacterial growth phase, to cite only a few parameters (Travassos et al., 2004). The ability of the PGN to serve as a ligand for its host receptor also depends on other cell wall components such as teichoic acid but also on PGN degrading enzymes such as amidase or lysozymes that degrade it

(Vaz et al., 2019). It is therefore complicated to speculate on what could be a physiological concentration of PGN for flies sensing its environment.

Thus, in nature, PGN is likely detected in combination with other tastants and odorants, which detected alone may lead to an array of conflicting behaviors but in combination will yield one context-dependent behavioral output (Soldano et al., 2016; Lopez-Requena et al., 2017). Consequently, it may be hazardous to expect clear phenotypes, or to make sense of the observed ones for the ecology of the fly when testing a single molecule of the permanent environment of the animal while this molecule is not especially deleterious per se but rather informative for the insect. The PGN is an interesting case as, on the one hand, an internal sensing of this molecule indicates an infection, the uncontrolled growth of a bacteria, or a breach in a physical barrier. On the other hand, the perception of this same molecule in the environment might be a clue, among others, to suggest a heavily contaminated place.

## References


Aranha MM, Vasconcelos ML (2018) Deciphering *Drosophila* female innate behaviors. Curr Opin Neurobiol 52:139–148.

Buchon N, Silverman N, Cherry S (2014) Immunity in *Drosophila melanogaster*—from microbial recognition to whole-organism physiology. Nat Rev Immunol 14:796–810.

Charroux B, Capo F, Kurz CL, Peslier S, Chaduli D, Viallat-Lieutaud A, Royet J (2018) Cytosolic and secreted peptidoglycan-degrading enzymes in *Drosophila* respectively control local and systemic immune responses to microbiota. Cell Host Microbe 23:215–228.e4.

Chen YD, Dahanukar A (2020) Recent advances in the genetic basis of taste detection in *Drosophila*. Cell Mol Life Sci 77:1087–1101.

De Gregorio E, Spellman PT, Tzou P, Rubin GM, Lemaitre B (2002) The Toll and Imd pathways are the major regulators of the immune response in *Drosophila*. EMBO J 21:2568–2579.

Depetris-Chauvin A, Galagovsky D, Chevalier C, Maniere G, Grosjean Y (2017) Olfactory detection of a bacterial short-chain fatty acid acts as an orexigenic signal in *Drosophila melanogaster* larvae. Sci Rep 7:14230.

Dunipace L, Meister S, McNealy C, Amrein H (2001) Spatially restricted expression of candidate taste receptors in the *Drosophila* gustatory system. Curr Biol 11:822–835.

Fan P, Manoli DS, Ahmed OM, Chen Y, Agarwal N, Kwong S, Cai AG, Neitz J, Renslo A, Baker BS, Shah NM (2013) Genetic and neural mechanisms that inhibit *Drosophila* from mating with other species. Cell 154:89–102.

French A, Agha MA, Mitra A, Yanagawa A, Sellier MJ, Marion-Poll F (2015) *Drosophila* bitter taste(s). Front Integr Neurosci 9:58.

Gottar M, Gobert V, Michel T, Belvin M, Duyk G, Hoffmann JA, Ferrandon D, Royet J (2002) The *Drosophila* immune response against Gram-negative bacteria is mediated by a peptidoglycan recognition protein. Nature 416:640–644.

Guo L, Karpac J, Tran SL, Jasper H (2014) PGRP-SC2 promotes gut immune homeostasis to limit commensal dysbiosis and extend lifespan. Cell 156:109–122.

Hardie RC, Raghu P, Moore S, Juusola M, Baines RA, Sweeney ST (2001) Calcium influx via TRP channels is required to maintain PIP2 levels in *Drosophila* photoreceptors. Neuron 30:149–159.

Harris N, Braiser DJ, Dickman DK, Fetter RD, Tong A, Davis GW (2015) The innate immune receptor PGRP-LC controls presynaptic homeostatic plasticity. Neuron 88:1157–1164.

Harris N, Fetter RD, Brasier DJ, Tong A, Davis GW (2018) Molecular interface of neuronal innate immunity, synaptic vesicle stabilization, and presynaptic homeostatic plasticity. Neuron 100:1163–1179.e4.

Hedengren M, Asling B, Dushay MS, Ando I, Ekengren S, Wihlborg M, Hultmark D (1999) Relish, a central factor in the control of humoral but not cellular immunity in *Drosophila*. Mol Cell 4:827–837.

Hoffman C, Aballay A (2019) Role of neurons in the control of immune defense. Curr Opin Immunol 60:30–36.

Itskov PM, Moreira JM, Vinnik E, Lopes G, Safarik S, Dickinson MH, Ribeiro C (2014) Automated monitoring and quantitative analysis of feeding behaviour in *Drosophila*. Nat Commun 5:4560.

Kaneko T, Yano T, Aggarwal K, Lim JH, Ueda K, Oshima Y, Peach C, Erturk-Hasdemir D, Goldman WE, Oh BH, Kurata S, Silverman N (2006) PGRP-LC and PGRP-LE have essential yet distinct functions in the *Drosophila* immune response to monomeric DAP-type peptidoglycan. Nat Immunol 7:715–723.

Kavaliers M, Ossenkopp KP, Choleris E (2020) Pathogens, odors, and disgust in rodents. Neurosci Biobehav Rev 119:281–293.

Khush RS, Cornwell WD, Uram JN, Lemaitre B (2002) A ubiquitin-proteasome pathway represses the *Drosophila* immune deficiency signaling cascade. Curr Biol 12:1728–1737.

Kim H, Kim H, Kwon JY, Seo JT, Shin DM, Moon SJ (2018) *Drosophila* Gr64e mediates fatty acid sensing via the phospholipase C pathway. PLoS Genet 14:e1007229.

Kobler JM, Rodriguez Jimenez FJ, Petcu I, Grunwald Kadow IC (2020) Immune receptor signaling and the mushroom body mediate post-ingestion pathogen avoidance. Curr Biol 30:4693–4709.e3.

Kurata S (2014) Peptidoglycan recognition proteins in *Drosophila* immunity. Dev Comp Immunol 42:36–41.

Kurz CL, Charroux B, Chaduli D, Viallat-Lieutaud A, Royet J (2017) Peptidoglycan sensing by octopaminergic neurons modulates Drosophila oviposition. Elife 6:e21937.

Kwon JY, Dahanukar A, Weiss LA, Carlson JR (2014) A map of taste neuron projections in the Drosophila CNS. J Biosci 39:565–574.

Lee KZ, Ferrandon D (2011) Negative regulation of immune responses on the fly. EMBO J 30:988–990.

Leulier F, Rodriguez A, Khush RS, Abrams JM, Lemaitre B (2000) The *Drosophila* caspase Dredd is required to resist gram-negative bacterial infection. EMBO Rep 1:353–358.

Leulier F, Parquet C, Pili-Floury S, Ryu JH, Caroff M, Lee WJ, Mengin-Lecreulx D, Lemaitre B (2003) The *Drosophila* immune system detects bacteria through specific peptidoglycan recognition. Nat Immunol 4:478–484.

Lindsay SA, Wasserman SA (2014) Conventional and non-conventional *Drosophila* Toll signaling. Dev Comp Immunol 42:16–24.

Liu W, Zhang K, Li Y, Su W, Hu K, Jin S (2017) Enterococci mediate the oviposition preference of *Drosophila melanogaster* through sucrose catabolism. Sci Rep 7:13420.

Lopes G, Bonacchi N, Frazao J, Neto JP, Atallah BV, Soares S, Moreira L, Matias S, Itskov PM, Correia PA, Medina RE, Calcaterra L, Dreosti E, Paton JJ, Kampff AR (2015) Bonsai: an event-based framework for processing and controlling data streams. Front Neuroinform 9:7.

Lopez-Requena A, Boonen B, Van Gerven L, Hellings PW, Alpizar YA, Talavera K (2017) Roles of neuronal TRP channels in neuroimmune interactions. In: Neurobiology of TRP channels (Emir TLR, ed), pp. 1–18. Boca Raton, FL: CRC.

Maillet F, Bischoff V, Vignal C, Hoffmann J, Royet J (2008) The *Drosophila* peptidoglycan recognition protein PGRP-LF blocks PGRP-LC and IMD/JNK pathway activation. Cell Host Microbe 3:293–303.

Marella S, Fischler W, Kong P, Asgarian S, Rueckert E, Scott K (2006) Imaging taste responses in the fly brain reveals a functional map of taste category and behavior. Neuron 49:285–295.

Martino ME, Ma D, Leulier F (2017) Microbial influence on *Drosophila* biology. Curr Opin Microbiol 38:165–170.

Masuzzo A, Maniere G, Viallat-Lieutaud A, Avazeri E, Zugasti O, Grosjean Y, Kurz CL, Royet J (2019) Peptidoglycan-dependent NF-kappaB activation in a small subset of brain octopaminergic neurons controls female oviposition. Elife 8:e50559.

Masuzzo A, Montanari M, Kurz L, Royet J (2020) How bacteria impact host nervous system and behaviors: lessons from flies and worms. Trends Neurosci 43:998–1010.

Mburu DM, Ochola L, Maniania NK, Njagi PG, Gitonga LM, Ndung'u MW, Wanjoya AK, Hassanali A (2009) Relationship between virulence and repellency of entomopathogenic isolates of *Metarhizium anisopliae* and *Beauveria bassiana* to the termite *Macrotermes michaelseni*. J Insect Physiol 55:774–780.

Min S, Ai M, Shin SA, Suh GS (2013) Dedicated olfactory neurons mediating attraction behavior to ammonia and amines in *Drosophila*. Proc Natl Acad Sci U S A 110:E1321–9.

Mishra D, Miyamoto T, Rezenom YH, Broussard A, Yavuz A, Slone J, Russell DH, Amrein H (2013) The molecular basis of sugar sensing in *Drosophila* larvae. Curr Biol 23:1466–1471.

Montell C (2009) A taste of the *Drosophila* gustatory receptors. Curr Opin Neurobiol 19:345–353.

Myllymaki H, Valanne S, Ramet M (2014) The *Drosophila* imd signaling pathway. JI 192:3455–3462.

Paredes JC, Welchman DP, Poidevin M, Lemaitre B (2011) Negative regulation by amidase PGRPs shapes the *Drosophila* antibacterial response and protects the fly from innocuous infection. Immunity 35:770–779.

Royet J, Gupta D, Dziarski R (2011) Peptidoglycan recognition proteins: modulators of the microbiome and inflammation. Nat Rev Immunol 11:837–851.

Sayin S, Boehm AC, Kobler JM, De Backer JF, Grunwald Kadow IC (2018) Internal state dependent odor processing and perception-the role of neuromodulation in the fly olfactory system. Front Cell Neurosci 12:11.

Silbering AF, Bell R, Galizia CG, Benton R (2012) Calcium imaging of odor-evoked responses in the *Drosophila* antennal lobe. J Vis Exp 2012:2976.

Soldano A, Alpizar YA, Boonen B, Franco L, Lopez-Requena A, Liu G, Mora N, Yaksi E, Voets T, Vennekens R, Hassan BA, Talavera K (2016) Gustatory-mediated avoidance of bacterial lipopolysaccharides via TRPA1 activation in *Drosophila*. Elife 5:e13133.

Stanley M, Ghosh B, Weiss ZF, Christiaanse J, Gordon MD (2021) Mechanisms of lactic acid gustatory attraction in *Drosophila*. Curr Biol 31:3525–3537.e6.

Stensmyr MC, Dweck HK, Farhan A, Ibba I, Strutz A, Mukunda L, Linz J, Grabe V, Steck K, Lavista-Llanos S, Wicher D, Sachse S, Knaden M, Becher PG, Seki Y, Hansson BS (2012) A conserved dedicated olfactory circuit for detecting harmful microbes in *Drosophila*. Cell 151:1345–1357.

Stoven S, Ando I, Kadalayil L, Engstrom Y, Hultmark D (2000) Activation of the *Drosophila* NF-kappaB factor Relish by rapid endoproteolytic cleavage. EMBO Rep 1:347–352.

Sullivan K, Fairn E, Adamo SA (2016) Sickness behaviour in the cricket *Gryllus texensis*: comparison with animals across phyla. Behav Processes 128:134–143.

Swanson JA, Torto B, Kells SA, Mesce KA, Tumlinson JH, Spivak M (2009) Odorants that induce hygienic behavior in honeybees: identification of volatile compounds in chalkbrood-infected honeybee larvae. J Chem Ecol 35:1108–1116.

Takehana A, Yano T, Mita S, Kotani A, Oshima Y, Kurata S (2004) Peptidoglycan recognition protein (PGRP)-LE and PGRP-LC act synergistically in *Drosophila* immunity. EMBO J 23:4690–4700.

Thistle R, Cameron P, Ghorayshi A, Dennison L, Scott K (2012) Contact chemoreceptors mediate male-male repulsion and male-female attraction during *Drosophila* courtship. Cell 149:1140–1151.

Thorne N, Chromey C, Bray S, Amrein H (2004) Taste perception and coding in *Drosophila*. Curr Biol 14:1065–1079.

Travassos LH, Girardin SE, Philpott DJ, Blanot D, Nahori MA, Werts C, Boneca IG (2004) Toll-like receptor 2-dependent bacterial sensing does not occur via peptidoglycan recognition. EMBO Rep 5:1000–1006.

Vaz F, Kounatidis I, Covas G, Parton RM, Harkiolaki M, Davis I, Filipe SR, Ligoxygakis P (2019) Accessibility to peptidoglycan is important for the recognition of Gram-positive bacteria in *Drosophila*. Cell Rep 27:2480–2492.e6.

Wang Z, Singhvi A, Kong P, Scott K (2004) Taste representations in the *Drosophila* brain. Cell 117:981–991.

Weiss LA, Dahanukar A, Kwon JY, Banerjee D, Carlson JR (2011) The molecular and cellular basis of bitter taste in *Drosophila*. Neuron 69:258–272.

Yanagawa A, Neyen C, Lemaitre B, Marion-Poll F (2017) The gram-negative sensing receptor PGRP-LC contributes to grooming induction in *Drosophila*. PLoS One 12:e0185370.

You H, Lee WJ, Lee WJ (2014) Homeostasis between gut-associated microorganisms and the immune system in *Drosophila*. Curr Opin Immunol 30:48–53.

Zhai Z, Boquete JP, Lemaitre B (2018a) Cell-specific Imd-NF-kappaB responses enable simultaneous antibacterial immunity and intestinal epithelial cell shedding upon bacterial infection. Immunity 48:897–910.e7.

Zhai Z, Huang X, Yin Y (2018b) Beyond immunity: the Imd pathway as a coordinator of host defense, organismal physiology and behavior. Dev Comp Immunol 83:51–59.